2005

Autonomous optical measurements in Bayboro Harbor (Saint Petersburg, Florida)

Chunzi Du
University of South Florida

Autonomous Optical Measurements in Bayboro Harbor (Saint Petersburg, Florida)

by

Chunzi Du

A thesis submitted in partial fulfillment
of the requirements for the degree of
Master of Science
College of Marine Science
University of South Florida

Major Professor: Kendall L. Carder, Ph.D.
Gabriel A. Vargo, Ph.D.
Edward Van Vleet, Ph.D.

Date of Approval:
November 15, 2005

Keywords: Backscatter, Light Absorption, Phytoplankton, Remote Sensing

ACKNOWLEDGEMENTS

There are many people I would like to thank who have supported me greatly in one way or another during my study in the College of Marine Science. First and foremost, I would like to thank my advisor Dr. Kendall Carder for sharing with me his passion for ocean optics, providing me the opportunity to learn my own interests, and patiently offering encouragement. I would also like to thank my committee members, Dr. Gabriel Vargo and Dr. Edward Van Vleet, for their support and guidance. Their classes were instrumental in providing me with the biological and chemical framework necessary to interpret my optical findings. My husband and sons, I thank for providing balance to my life outside of the lab, so that I could put things into perspective.

My fellow lab mates were also very supportive and deserve many thanks. My friend Jennifer Cannizzaro has helped me in countless ways. She taught me how to operate the *in situ* optical sensors, helped with data collection and processing and supplied helpful editorial comments. David English kindly helped me with data sampling and instruments. Jim Ivey helped me with programming issues.

Financial support for this work was provided by NASA (NAS5-31716) and ONR (N00014-97-1-0006 and N00014-96-1-5013) funding.

TABLE OF CONTENTS

LIST OF TABLES

LIST OF FIGURES

Autonomous Optical Measurements in Bayboro Harbor

Chunzi Du

ABSTRACT

Estimating with precision coastal marine properties such as primary production, particulate and dissolved carbon, and red tide concentrations is a challenging but important part of marine research. It benefits not only the local communities, but also provides an important input to various global biogeochemical modeling efforts. Due to the complexity of coastal environments resulting from temporal variability of tidal and riverine influences, it is useful to develop and deploy an automated sensor network that provides real-time feedback. It can be used to validate remote sensing models to retrieve in-water constituents, and provide calibration and validation for atmospheric correction of satellite sensors. For turbid waters, satellite observations in the infrared part of the spectrum can not be used to estimate atmospheric aerosol concentration because the water is not “black” as is found for clearer waters. This research contribution introduces a modeling effort for a turbid coastal harbor area using a semi-analytical hyperspectral remote sensing algorithm for Case 2 waters to process data from the Autonomous Marine Optical System (AMOS). Retrieved results are then compared with field sample measurements showing satisfactory closure between measurements and theory. A time series of AMOS data over a one-month time span is examined, revealing significant

variations in biological activity. A sensitivity analysis of the model is performed to expose the limitations and possible improvements to AMOS measurements in the future.

1. INTRODUCTION

1.1 Background

Global climate change is becoming an increasingly discussed topic due to the huge impact it has on our daily lives. Although associations between global warming and regional climate patterns such as frequency and magnitude of hurricanes in the Atlantic Ocean have yet to be established, the need for better understanding of carbon cycles on global scales is evident. To support such tasks, traditional field spot-type sampling of oceanic environment will not be sufficient. Observations from space with sensors onboard satellites or aircraft will provide the only synoptic coverage with sufficient temporal and spatial resolution that can be used in analytical models for predictions [e.g. *Esaias et al.*, 1998] of global primary productivity and dissolved organic carbon fluxes from rivers.

Less than 10% of the light measured by a satellite ocean color sensor originates from beneath the ocean surface. The majority of received light is due to atmospheric absorption and scattering. Consequently, accurate atmospheric correction is critical in remote sensing applications since a small mistake will result in large errors when estimating correct water leaving radiances. The performance of retrieval algorithms and the accuracy of derived quantities are strongly influenced by atmospheric corrections.

Atmospheric correction algorithms have to cope with the reality in coastal waters that infrared wavebands treated as “atmospheric only” in open-ocean waters may contain

a non-negligible and variable signal from the sea as well. Classical atmospheric correction schemes assume that the water-leaving radiance is zero in the near-infrared part of the spectrum [*Gordon and Wang*, 1994]. However, recent experiences with space-borne data (e.g. SeaWiFS and MODIS) and ship-based optical measurements, clearly indicate that this assumption is not valid over turbid coastal waters [*Hu et al.*, 2000; *Siegel et al.*, 2000]. The principle contributing factor is high concentrations of scattering constituents that cause the water-leaving signal in the near-infrared part of the spectrum (>700nm) to be significantly greater than zero (i.e. not "black"). Therefore, it is highly desirable to have the ability to provide ground truth for atmospheric correction of satellite ocean color imagery. A network of autonomous optical sensors that measure downwelling irradiance and water-leaving radiance just above the sea surface may provide the necessary ground truth data to improve atmospheric corrections of coastal satellite ocean color data.

Derivation of in-water optical properties (e.g. absorption, backscattering, and chlorophyll concentrations) from water-leaving radiance data requires accurate processing algorithms. Using the spectral information from the light reflected from beneath the sea surface or the water-leaving radiance ($L_w(\lambda)$), many in-water properties have been successfully retrieved empirically or analytically, including diffuse attenuation coefficients [*Austin and Petzold*, 1981; *Stumpf and Pennock*, 1991], chlorophyll concentrations [*Carder et al.*, 1999; *Gordon et al.*, 1983; *O'Reilly et al.*, 1998], mass concentrations of suspended sediments [*Bukata et al.*, 1991; *Doerffer and Fisher*, 1994], and bottom depths for waters shallower than ~30 m [*Lee et al.*, 1999, 2001]. These properties can provide important input assessing the status of the water environment

[*Jerlov*, 1976], and help to better understand the oceanic photosynthetic process[*Kirk*, 1994; *Marra et al.*, 1992; *Platt and Sathyendranath*, 1988], as well as heat transfer [*Lewis et al.*, 1990; *Morel and Antoine*, 1994].

The initial success of the coastal zone color scanner (CZCS, 1978-1986) chlorophyll algorithm [*Gordon et al.*, 1983] profoundly enriched our knowledge of the global distribution of phytoplankton, especially in the open ocean environments [*Mitchell*, 1994]. A better understanding of in-water optical properties later led to improved algorithms for a series of next-generation sensors, such as the widely-used Sea-viewing Wide Field-of-View sensor (SeaWiFS, 1997-present) and Moderate-Resolution Imaging Spectrometer (MODIS).

To provide better quantification models to interpret remotely sensed signals, two water types namely Case 1 and Case 2, were introduced by Morel and Prieur, [1977], and refined later by Gordon and Morel, [1983]. By definition, Case 1 waters are those waters in which phytoplankton is the principle agent responsible for variations in optical properties of the water, while Case 2 waters are influenced not just by phytoplankton and related particles, but also by other substances that vary independently of phytoplankton (e.g. inorganic particles in suspended state and colored dissolved organic matter, CDOM, or gelbstoff). Case 1 waters are often found in the open ocean where influences from the land and seafloor are minimal. This type of water covers most of the oceanic environment (up to 90%). However, they are usually less productive compared to the Case 2 type coastal waters.

Due to the fact that Case 2 waters are primarily characterized by several optically-active substances which vary independently of each other and in many cases, are

accompanied by relatively high levels of scattering, algorithms developed for Case 1 waters can not be applied to Case 2 waters [*Carder et al.*, 1986, 1991]. Many commonly-used algorithms for Case 1 waters are based on correlations between some simple function of ocean-color signals at two or three wavebands and chlorophyll *a* concentration [*Gordon et al.*, 1983; *Morel and Prieur*, 1977]. Different algorithms are required for Case 2 water types because there are more optical components influencing the measured spectra. Also, due to the overlapping of absorption and scattering spectra, variations in radiance or reflectance can not be related directly to any one component, and the contributions by individual constituents have to be derived simultaneously [*Neumann et al.*, 2000]. Lastly, in shallow coastal regions and harbor areas with water depth less than 30m, bottom reflection effects may have to be included in the algorithms. Such complications imply no generic algorithms for all Case 2 water types will work. Instead, individual models and algorithms may have to be developed to meet needs for specific regions.

In recent years, hyperspectral remote sensing has gained much attention, especially in Case 2 water applications, and has revealed subtle information that was previously undiscovered. For example, spectral signatures of different phytoplankton classes or species can be found from hyperspectral sensors [*Bidigare et al.*, 1989; *Hoepffner and Sathyendranath*, 1993; *Millie et al.*, 1997]. A semi-analytical (SA) model was developed by Lee et al. [1998] for hyperspectral remote sensing needs. Briefly, the Lee et al. [1998] SA model provides accurate results comparable to Monte Carlo simulation and Hydrolight approaches but with much less computational needs. In the mean time, the SA model allows quick inversion of in-water constituents, including

bottom effects [*Lee et al.*, 1999]. Also, because of the fact that the SA model is not strongly dependent on choices of scattering phase functions, it is best suited for use with Case 2 water types, especially in a very turbid environment like Bayboro Harbor (St. Petersburg, FL).

1.2 Objectives and Approach

The west Florida shelf (WFS) has been selected by many agencies as a study site for long-term monitoring by instrumented platforms and underwater vehicles, aircraft, spacecraft, and monthly ship surveys. It is a region where numerical models of circulation and phytoplankton dynamics are being developed. An array of automated, continuous sensors could provide investigators with a continuous record of optical conditions during rapidly changing events such as storms, plankton blooms, tidal flushing, and upwelling. They can also provide boundary conditions for the bio-optical models being developed for predicting primary production and optical properties for the WFS and provide optical data to calibrate and explain variations in satellite imagery. From an economics view point, it is rather expensive and unpractical to deploy a research vessel at a fixed location for extended periods of time for monitoring purposes. From a research point of view, an autonomous array of sensors could greatly enhance our understanding of river blooms and the temporal variability of red tides [*Cannizzaro et al.*, 2002].

The Autonomous Marine Optical System (AMOS) was developed at the University of South Florida to measure hyperspectral remote-sensing reflectance spectra and water column measurements of downwelling irradiance, backscattering, beam

attenuation, and chlorophyll fluorescence. It was deployed in Bayboro Harbor (Saint Petersburg, Florida) intermittently between May of 2004 and July 2005.

The primary hypothesis of this research is that by carefully adjusting model parameters, the semi-analytical hyperspectral remote-sensing model by Lee et al. [1999] can be used to successfully retrieve in-water optical properties (e.g. phytoplankton absorption ($a_{ph}(\lambda)$), gelbstoff absorption ($a_g(\lambda)$) and particle backscattering ($b_{bp}(\lambda)$) from above-water remote-sensing measurements in turbid coastal environments. It is expected that new model parameters will be needed for this very turbid type of water, and parameters derived from the west Florida shelf will not perform as well. $R_{rs}(\lambda)$ data collected using a 512-channel, hand-held radiometer (Spectrix) is used for this purpose. The secondary hypothesis is that AMOS provides accurate $R_{rs}(\lambda)$ data, comparable to that from Spectrix measurements. A validation analysis is performed. Lastly, the improved $R_{rs}(\lambda)$ model modified to perform accurately in Bayboro Harbor is applied to validated AMOS $R_{rs}(\lambda)$ data, and a monthly time series is examined.

2. DATA AND METHODS

2.1 Study area

AMOS was developed with funding by the Defense University Research Instrumentation Program (DURIP) and was originally deployed near Port Manatee in Tampa Bay [*Steward and Carder*, 2002]. For this study, it was placed in Bayboro Harbor (Saint Petersburg, Florida) on a piling located on the southeast corner of the USF College of Marine Science (CMS) (Fig.1). Bayboro Harbor comprises two connected basins with

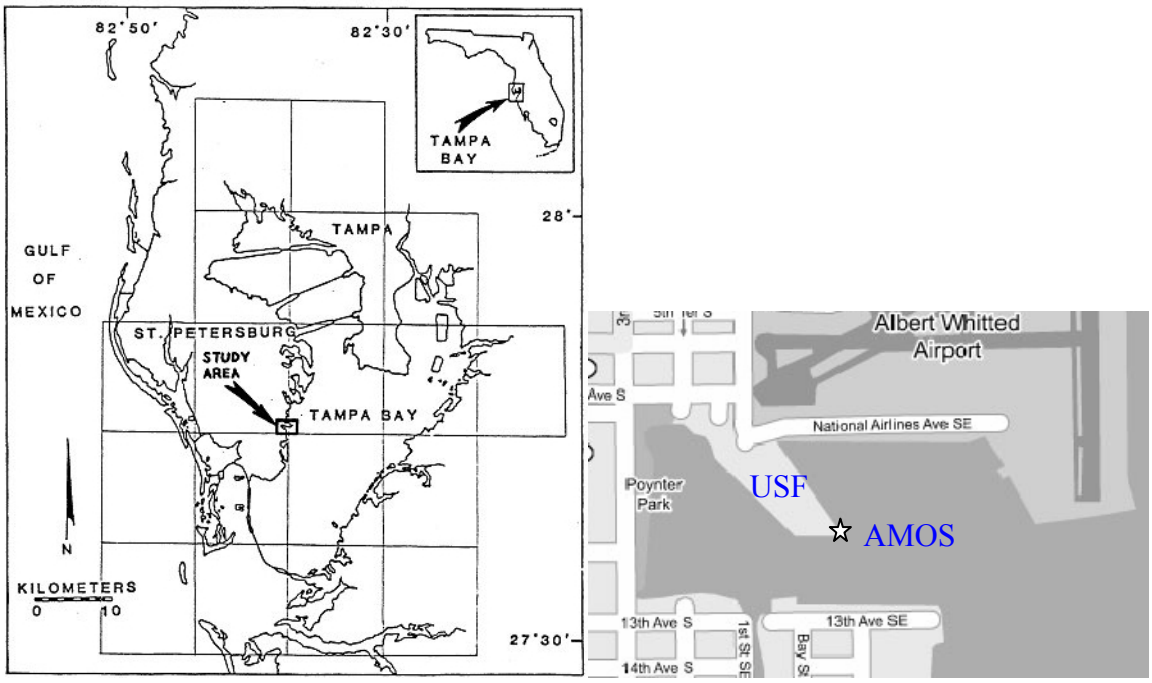

Figure 1. AMOS sampling location in Bayboro Harbor (St. Petersburg, FL).

an average depth of 6 meters. It is bounded on three sides by developed shoreline. Both basins are connected to Tampa Bay through a narrow dredged shipping channel of 7.3m depth. These basins receive storm water runoff (largely from Salt Creek), and nearby facility discharges, such as from U. S. Coastal Guard St. Petersburg Station, Albert Whitted Municipal Airport, and City of St. Petersburg's Municiple Sewage Treatment Plant. The two basins are separated by an extrusion of land that contains buildings of the University of South Florida College of Marine Science (Fig. 1). The site was chosen in order to measure Case 2 waters in a location easily accessible for routine maintenance and collection of validation data.

2.2 AMOS

AMOS was built in 2000 by the Center for Ocean Technology (COT) of the University of South Florida (USF) as a prototype sampling device. At predetermined times, it make remote sensing reflectance ($R_{rs}(\lambda)$) measurements above the water surface as well as in-water measurements of optical properties at one or more depths. After sampling, it transmits the information back to a networked archival and processing station. Note that symbol definitions can be found in Table 1.

The AMOS installation is composed of a power supply, a master controller, an above-water remote-sensing radiometer, and an in-water sub-controller for an underwater $E_d(\lambda)$ sensor and inherent optical property (IOP) instruments (Fig. 2). A solar panel recharges the battery power supply, so that neither power, nor communication cables are needed between AMOS and the shore. At scheduled times throughout the day (Table 2) AMOS measures down-welling irradiance, upwelling sky radiance, irradiance at depth,

Table 1. Symbol definitions

Symbols	Description	Units
A	Absorption coefficient ($=a_w+a_{ph}+a_d+a_g$)	m^{-1}
a_w	Absorption coefficient of pure water	m^{-1}
a_p	Absorption coefficient of particulates ($=a_{ph}+a_d$)	m^{-1}
a_{ph}	Absorption coefficient of phytoplankton	m^{-1}
a_d	Absorption coefficient of detritus	m^{-1}
a_g	Absorption coefficient of gelbstoff	m^{-1}
A	Empirical shape coefficient for power law function ($y=Ax^B$)	
b_b	Backscattering coefficient	m^{-1}
b_{bw}	Backscattering coefficient of pure water	m^{-1}
b_{bp}	Backscattering coefficient of particulates	m^{-1}
b_p	Scattering coefficient of particles	m^{-1}
B	Empirical slope coefficient for power law function ($y=Ax^B$)	
c	Attenuation coefficient	m^{-1}
Chl	Chlorophyll *a* concentration	mg m^{-3}
E_d	Downwelling irradiance	W m^{-2} nm^{-1}
f	Water-to-air divergence factor	
FLH	Fluorescence line height	W m^{-2} μm^{-1} sr^{-1}
L_G	Radiance reflected from a 10% diffuse reflector or gray card	
L_{sky}	Downwelling sky radiance	W m^{-2} nm^{-1} sr^{-1}
L_u	Upwelling radiance	W m^{-2} nm^{-1} sr^{-1}
L_w	Water-leaving radiance	W m^{-2} nm^{-1} sr^{-1}
N	Refractive index of seawater	
nL_w	Normalized water-leaving radiance	W m^{-2} nm^{-1} sr^{-1}
Q	Upwelling irradiance-to-radiance ratio	sr^{-1}
R	Fresnel reflectance	
R_G	Reflectance of a 10% diffuse reflector or gray card	
R_{rs}	Above surface remote-sensing reflectance	sr^{-1}
r_{rs}	Subsurface remote-sensing reflectance	sr^{-1}
S_d	Spectral slope for detrital absorption spectra	m^{-1}
S_g	Spectral slope for gelbstoff absorption spectra	m^{-1}
T	Transmittance across the air-sea interface	
γ	Angstrom exponent describing spectral shape of $b_{bp}(\lambda)$	

chlorophyll fluorescence, attenuation of blue and red light (470 and 660nm), backscattering of blue and red light (470 and 676nm), and the Global Positioning System (GPS) location and time of sampling. This information is recorded on site and transmitted by radio to a computer at USF where it is archived and processed to customary scientific units.

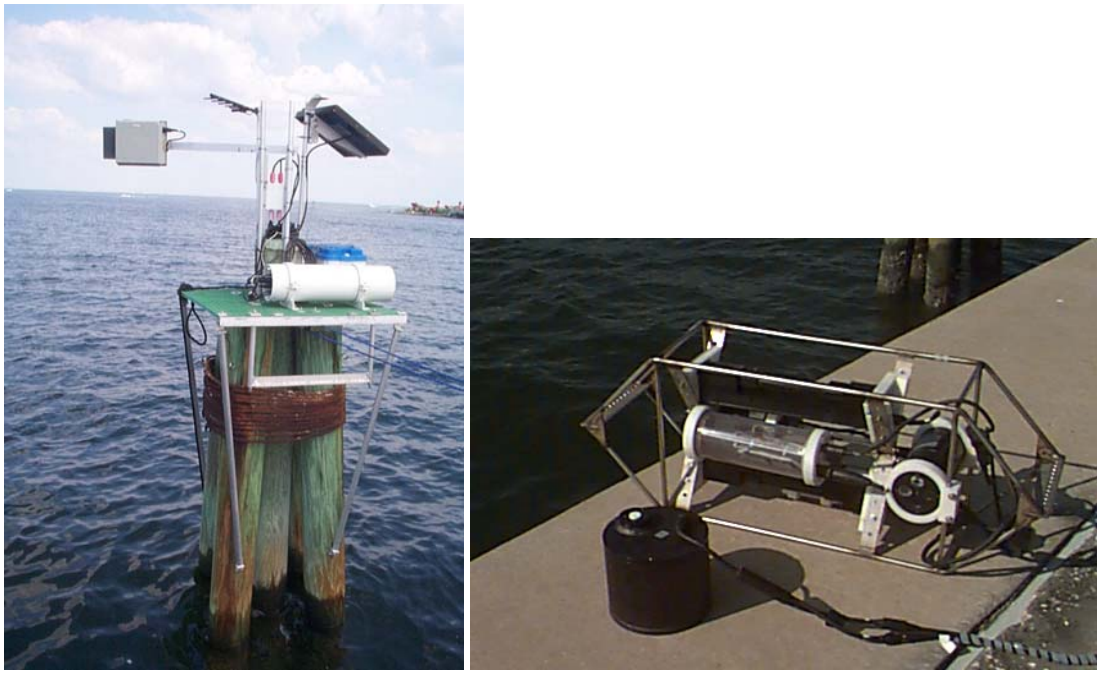

Figure 2. Left: AMOS above-water unit with extending radiometer, solar panel, and rechargeable battery pack; Right: AMOS underwater unit with fluorometer, transmissometers and back-scattering meters.

Table 2. AMOS sampling schedule.

Sampling time (EST)	No. samples
1:30~10:30 sampling every 3 hours	4
10:30~11:30 sampling every half hour	2
11:30~15:00 sampling every 15 min	14
15:30 sampling	1
16:30 sampling	1
19:30 sampling	1
23:30 sampling	1

2.3 Remote-sensing reflectance, $R_{rs}(\lambda)$

2.3.1 AMOS radiometer

The automated measurement of $R_{rs}(\lambda)$ using a single radiometer that looks at multiple optical pathways is an important feature of AMOS. A fiber-optic switch allows measurement of the light from a down-welling cosine collector, a sea-surface viewing window, a complementary-angle sky-viewing window, or a terminated light path (to measure dark current). This single spectrometer arrangement allows $R_{rs}(\lambda)$ spectral ratios to be made without distortions from sharp spectral features such as Fraunhofer lines. The radiance windows are inclined so that the center view through these windows is 30° from the vertical, similar to the viewing angle that has been used with handheld spectrometers for several years [e.g. *Carder and Steward*, 1985].

Remote-sensing reflectance ($R_{rs}(\lambda)$) by AMOS is by definition

$$R_{rs}(AMOS,\lambda) = \frac{L_w(\lambda)}{E_d(\lambda)} \tag{1}$$

Light transmitted through the downwelling cosine collector provides the spectrometer a direct measurement of downwelling irradiance ($E_d(\lambda)$). This is followed by a spectrometric measure of the water upwelling radiance ($L_u(\lambda)$), and a measure of the sky downwelling radiance ($L_{sky}(\lambda)$). Combining these generates water leaving radiance ($L_w(\lambda)$),

$$R_{rs}(\lambda) = T_{rs}(\lambda) - 0.022 * S_{rs}(\lambda) = \frac{L_u(\lambda)}{E_d(\lambda)} - 0.022 * \frac{L_{sky}(\lambda)}{E_d(\lambda)} \tag{2}$$

The effect of skylight on this "measured" remote sensing reflectance is removed by a factor of 0.022, which is the contribution of Fresnel reflectance for a 30^o viewing angle [*Mobley*, 1994].

2.3.2 Spectrix radiometer

A hand-held, 512-channel spectroradiometer (Spectrix, 350~850nm) (Fig. 3a) was used to measure $L_u(\lambda)$ (upwelling radiance), $L_G(\lambda)$ (radiance reflected from a standard grey diffuse reflector) and $L_{sky}(\lambda)$ (sky radiance) at Bayboro Harbor intermittently from May 2004 to July 2005 (~1-2 times per week) when AMOS was deployed. These measurements were used to estimate $E_d(\lambda)$ and $L_w(\lambda)$. The ratio of $L_w(\lambda)$ and $E_d(\lambda)$ then provided the remote-sensing reflectance [*Lee et al.*, 1996].

2.4 Absorption

Absorption spectra due to particles (phytoplankton and detritus), $a_p(\lambda)$ were determined using the quantitative filter technique [*Kiefer and SooHoo*, 1982; *Yentsch*, 1962]. Seawater samples collected by bucket within 5 minutes of Spectrix radiance measurements were filtered through 2.5cm GF/F filters. The sample filter and a reference filter wetted with Milli Q water were placed on individual glass plates (diameter=2.4cm) in a custom-made diffuse transmissometer box. The transmittance of the sample filter, $T_{sample}(\lambda)$, and the reference filter, $T_{reference}(\lambda)$, were measured three times each using a custom-made, 512-channel spectroradiometer(~350-850nm).

Optical densities, OD(λ), were calculated as

$$OD(\lambda) = \log_{10}(\frac{T_{ref}(\lambda)}{T_{sample}(\lambda)}) \quad (3)$$

Particulate absorption spectra were calculated as

$$a_p(\lambda) = 2.3 * OD_p(\lambda) * \frac{\beta}{L} \quad (4)$$

where β is the optical path elongation or beta factor, and L is the effective optical pathlength (the area of filter pad divided by volume seawater filtered). The beta factor is an empirical formulation defined as the ratio of optical to geometric pathlength that corrects for multiple scattering inside the filter. In this study, an average of two published beta factor formulations [*Bricaud and Stramski*, 1990; *Nelson and Robertson*, 1993] was chosen

$$\beta = 1.0 + 0.6 * OD_p(\lambda)^{-0.5} \quad (5)$$

Phytoplankton pigments were extracted from the sample filter with ~20-50ml of hot 100% methanol for 10-15 minutes in the dark [*Kishino et al.*, 1985; *Roesler et al.*, 1989]. Fluorometric chlorophyll and pheopigment concentrations were determined using the filtrate using a Turner 10-AU-005 fluorometer (Fig. 3b) according to the methods of Holm-Hansen et al. [1965].

Light transmission was measured again on this extracted filter and the same reference filter to obtain the absorption spectra of detrital particles and non-methanol-extractable (e.g. water soluble) pigments, $a_d(\lambda)$. The absorption spectra for phytoplankton pigments, $a_{ph}(\lambda)$, is then calculated as

$$a_{ph}(\lambda) = a_p(\lambda) - a_d(\lambda) \quad (6)$$

Gelbstoff absorption spectra, $a_g(\lambda)$, were measured using filtered seawater obtained using pre-rinsed 0.2um nylon membrane filters. Samples are scanned in 10-cm quartz cells from 200-800nm, using a Perkin-Elmer Lambda 18 spectrophotometer (Fig. 3c) and referenced to Milli Q water.

Figure 3. Instruments for experiments: a) Spectrix: a 512-channel spectroradiometer; b) Turner 10-AU-005 fluorometer; c) Perkin-Elmer Lambda 18 spectrophotometer.

2.5 Backscattering

In situ vertical profiles of total backscattering measured at 470 and 676nm using a HOBI Labs Hydroscat2 (HS2) were performed on four occasions in May 2004. Measurement, calibration, and data processing information for this instrument have been described previously [*Maffione and Dana*, 1997]. A spectral power function was fit to measured backscattering values at 470 and 676nm in order to obtain the backscattering coefficient at 555nm. Particulate backscattering at 555nm, $b_{bp}(555)$, was calculated from total backscattering by subtracting the backscattering coefficient due to pure water [*Morel*, 1974].

3. THEORY

The semi-analytical (SA) model and optimization approach of Lee et al. [1998, 1999] retrieves in-water properties ($a_{ph}(\lambda)$, $a_g(\lambda)$, $b_{bp}(\lambda)$, water depth (H), and bottom albedo ($\rho(\lambda)$) from hyperspectral $R_{rs}(\lambda)$. A brief introduction of the SA model and optimization technique is described below.

For optically deep, vertically homogeneous waters, $R_{rs}(\lambda)$ is dependent on the absorption and backscattering properties of seawater and the angular distribution of light within the ocean. Using radiative transfer theory [*Gordon et al.*, 1988; *Mobley*, 1994], $R_{rs}(\lambda)$ can be expressed as

$$R_{rs}(\lambda) = \frac{t^2}{n^2} \frac{f}{Q(\lambda)} \frac{b_b(\lambda)}{a(\lambda) + b_b(\lambda)} \tag{7}$$

where t is the transmittance across the air-sea interface, n is the index of refraction of seawater, f is an empirical factor that is a function of the solar zenith angle, and $Q(\lambda)$ is the upwelling irradiance-to-radiance ratio, $a(\lambda)$ is the total absorption spectra, and $b_b(\lambda)$ is the total backscattering spectra.

By making approximations for these latter terms [*Lee et al.*, 1998], $R_{rs}(\lambda)$ can further be related to the subsurface remote-sensing reflectance, $r_{rs}(\lambda)$, as follows:

$$R_{rs}(\lambda) = \frac{0.5\, r_{rs}(\lambda)}{(1 - 1.5\, r_{rs}(\lambda))} \tag{8}$$

In optically shallow waters, contributions from the bottom can be expressed separately from deep water effects in terms of sub-surface remote sensing reflectance as [*Lee et al.*, 1999]

$$r_{rs} \approx r_{rs}^{dp}\left[1-\exp\left(-\left(\frac{1}{1.2}+\frac{D_u^{C}}{0.92}\right)\kappa H\right)\right]+\frac{1}{\pi}\rho\exp\left(-\left(\frac{1}{1.2}+\frac{D_u^{B}}{0.92}\right)\kappa H\right) \tag{9}$$

where r_{rs}^{dp} is the subsurface remote-sensing reflectance for optically deep waters, D_u^{C} is the optical-path-elongation factor due to multiple scattering for the water column, D_u^{B} is the optical-path-elongation factor for the bottom-reflected photons, and κ is equal to the sum of the absorption and backscattering coefficients.

For optically deep waters subsurface remote-sensing reflectance is [*Lee et al.*, 2004]

$$r_{rs}^{dp} = g_w \frac{b_{bw}}{a+b_b} + g_p \frac{b_{bp}}{a+b_b} \tag{10}$$

where g_w and g_p are known model-derived parameters for molecular and particle scattering, respectively. Separate terms for particles and molecules are required because the angular distribution for molecular backscattering due to water, $b_{bw}(\lambda)$, differs from that of particulate backscattering due to water.

Optical path elongation factors for the water column and bottom are [*Lee et al.*, 1999]

$$D_u^{C} \approx 1.03\left(1+2.4u\right)^{0.5} \text{ and } D_u^{B} \approx 1.04\left(1+5.4u\right)^{0.5} \tag{11}$$

respectively, where

$$u = \frac{b_b}{a+b_b} \tag{12}$$

The absorption coefficient can be examined more thoroughly by decomposing it into the sum of its components:

$$a(\lambda) = a_w(\lambda) + a_{ph}(\lambda) + a_d(\lambda) + a_g(\lambda) \quad (13)$$

where the subscripts w, ph, d, and g refer to water, phytoplankton, detritus and gelbstoff, respectively (Fig. 4). Similarly, the backscattering coefficient can be expanded as

$$b_b(\lambda) = b_{bw}(\lambda) + b_{bp}(\lambda) \quad (14)$$

where the subscripts w and p refer to water and particles (phytoplankton and detritus), respectively (Fig. 5). Absorption due to water, $a_w(\lambda)$, and backscattering due to water are constant and well known [*Morel*, 1974; *Pope and Fry*, 1997]. Terms for chlorophyll and gelbstoff fluorescence and water-Raman scattering are not included in this model. The water column is assumed to be homogeneous and the bottom a Lambertian reflector.

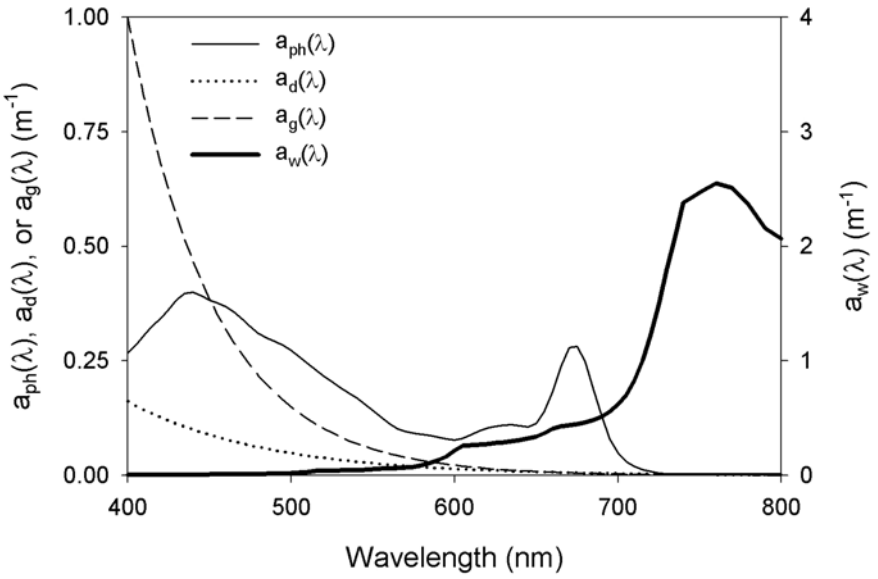

Figure 4. Examples of phytoplankton, detrital and gelbstoff absorption spectra and the absorption spectra due to pure water [*Pope and Fry,* 1997].

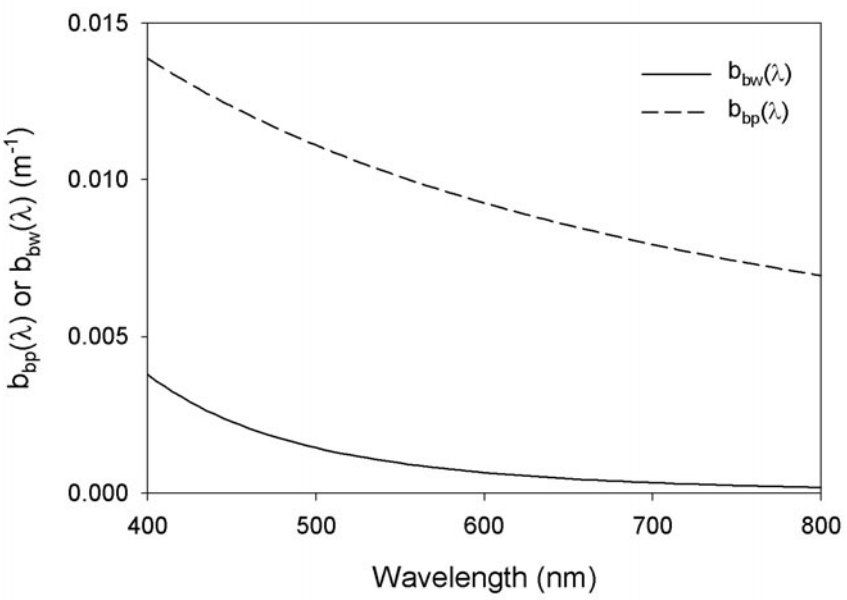

Figure 5. Example of particulate backscattering spectra and the backscattering spectra due to pure water [*Morel,* 1974].

Combining Eqs. (8-14) provide a model for deriving $a_{ph}(\lambda)$, $a_g(\lambda)$, $b_{bp}(\lambda)$, $\rho(\lambda)$ and H from $R_{rs}(\lambda)$. These terms are parameterized below in order to reduce the number of unknowns.

Phytoplankton absorption spectra are modeled from $a_{ph}(440)$ as [*Lee*, 1994]

$$a_{ph}(\lambda) = a_{ph}(440)\left[A_0(\lambda) + A_1(\lambda)\ln\left(a_{ph}(440)\right)\right] \tag{15}$$

where $A_0(\lambda)$ and $A_1(\lambda)$ are empirically derived constants. This function ensures that $a_{ph}(\lambda)$ curvature changes appropriately with $a_{ph}(440)$, taking into consideration the natural variability observed in phytoplankton pigmentation and pigment packaging [*Bricaud et al.*, 1995].

Absorption spectra due to gelbstoff is modeled from $a_g(440)$ as [*Lee et al.*, 1999]

$$a_g(\lambda) = a_g(440) * e^{-S(\lambda-440)} \tag{16}$$

where S is the spectral slope calculated for log-transformed absorption values. Since gelbstoff and detritus both exhibit exponentially decreasing absorption with increasing wavelength, they cannot be derived independently. Therefore, $a_g(\lambda)$ and $a_d(\lambda)$ are combined and an average spectral slope ($0.015 nm^{-1}$) is used [*Carder et al.*, 1989, 1991].

Particle backscattering spectra are modeled from $b_{bp}(555)$ as

$$b_{bp}(\lambda) = b_{bp}(555)\left(\frac{555}{\lambda}\right)^{Y} \tag{17}$$

where the reference wavelength 555nm replaces the 400nm value originally used by Lee et al. [1999]. The spectral shape parameter for backscattering, Y, is estimated using an empirical relationship from measured $R_{rs}(443)$ and $R_{rs}(490)$ data and values are limited to the 0-2.5 range [*Lee et al.*, 1999].

Bottom albedo spectra are expressed as

$$\rho(\lambda) = \rho(550) * \rho_{550nm-normalized}(\lambda) \tag{18}$$

where $\rho(550)$ is the bottom albedo coefficient at 550nm, and $\rho_{550nm\text{-}normalized}(\lambda)$ is a bottom albedo spectrum normalized at 550nm for sand [*Lee et al.*, 1999].

Since $R_{rs}(750)$ for turbid coastal waters may not be zero [*Hu et al.*, 2000; *Siegel et al.*, 2000], $R_{rs}^{in}(\lambda)$ is defined as

$$R_{rs}^{\ in} = R_{rs}^{\ meas} + \Delta \tag{19}$$

where R_{rs}^{meas} is the remote-sensing reflectance measured using either the AMOS or Spectrix radiometric sensors. The delta, Δ, factor is nonspectral (e.g. white) reflected

light representing residual sunglint, cloud light, and skylight brought into AMOS by wave facets and not removed by Eq. 2.

Values for $a_{ph}(440)$, $a_g(440)$, $b_{bp}(550)$, $\rho(550)$, H and Δ are then derived iteratively using a predictor-corrector optimization scheme until the difference between $R_{rs}(\lambda)_{in}$ and $R_{rs}(\lambda)_{mod.}$ is minimized [*Lee et al.*, 1999]. Parameter input values provided to the model are independent of field measurements.

4. RESULTS

4.1 Chlorophyll *a* concentration

Chlorophyll *a* concentrations in Bayboro Harbor measured during the study period range between 2.48 and 47.74 mg m^{-3}, with a mean value of 9.47 mg m^{-3} (Fig. 6).

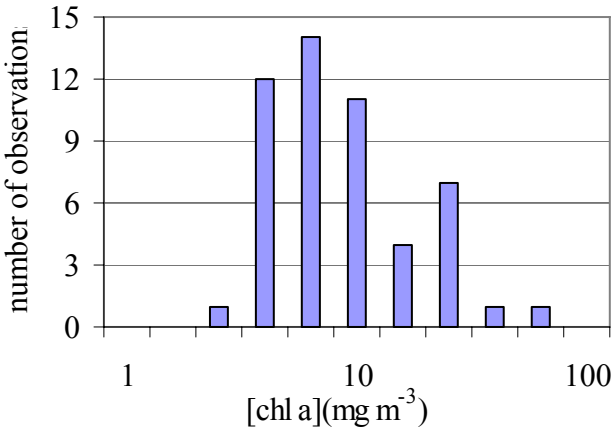

Figure 6. Distribution of chlorophyll *a* concentrations observed during this study period (May 2004 to July 2005) at Bayboro Harbor (Saint Petersburg, Florida).

This is in significant contrast to a recent West Florida shelf and Bahamas study where chlorophyll *a* concentrations ranged from 0.026 to 20.6 mg m^{-3}, with a mean value of 0.66 mg m^{-3} [*Cannizzaro and Carder*, 2005 (submitted)]. The higher mean chlorophyll concentrations observed in Bayboro Harbor indicates that this region is highly eutrophic indicating that perhaps a new set of model parameters for the SA model [*Lee et al.*, 1999] may be needed to adequately describe Bayboro Harbor.

4.2 Semi-analytic $R_{rs}(\lambda)$ model

Between May 2004 and July 2005, 45 remote-sensing reflectance spectra were collected using a Spectrix radiometer from Bayboro Harbor (Fig. 7). Maximal reflectance

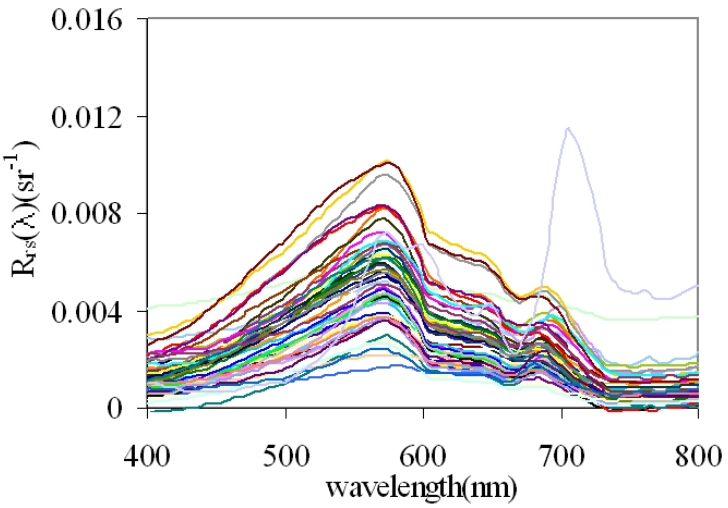

Figure 7. Remote-sensing reflectance spectral measurements collected during the study period (May 2004 to July 2005) from Bayboro Harbor. Measurements were obtained using a 512-channel spectral radiometer (Spectrix).

is typically observed around 570 nm which is why eutrophic harbor areas are usually "greenish" in color. A smaller peak around 685 nm is due to chlorophyll fluorescence. The anomalous curve with peak reflectance at ~700nm corresponds to a *K.brevis* bloom observed in July 2005 with a chlorophyll-*a* concentration of 71.9 mg m^{-3}. Since it is an isolated case and presents very different optical characteristics from typical in-water constituents in the harbor water, it is not included in this modeling effort.

The reflectance at the blue end (~400nm) is low due to the fact that chlorophyll and gelbstoff concentrations are high in the study area. A careful partition of signals at

this wavelength would help to better identify in-water constituents. At the longer wavelengths, especially beyond 700nm, reflectance values are low due to significantly higher water absorption values (Fig. 4).

4.2.1. Original model parameters

In order to determine how well the Lee et al. [1998, 1999] optimization technique works in Bayboro Harbor, the technique was first applied to Spectrix $R_{rs}(\lambda)$ data using the original model parameters derived from west Florida shelf data. Values for $a_{ph}(440)$, $a_g(440)$, $b_{bp}(555)$, $\rho(550)$, H and Δ were derived by minimizing the differences between measured and modeled $R_{rs}(\lambda)$ data. Figure 8 shows a few examples of these measured and

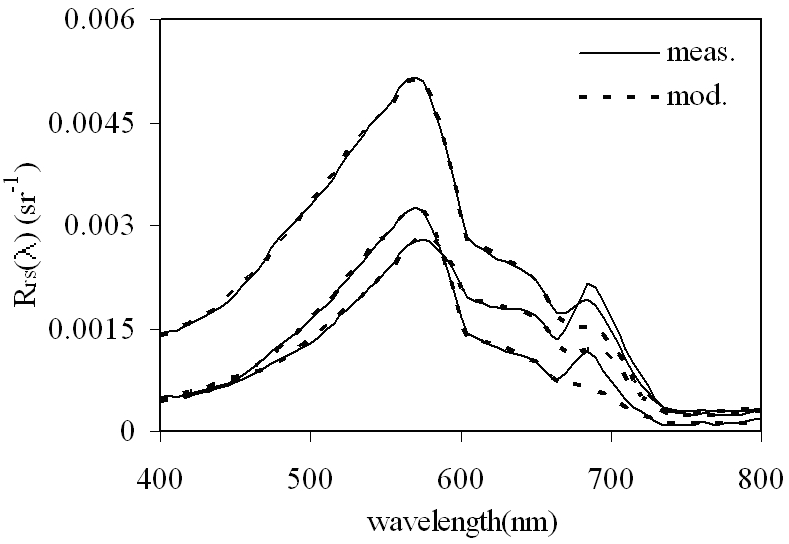

Figure 8. Selected modeled $R_{rs}(\lambda)$ curves derived by the original Lee et al.[1999] optimization model parameters compared to directly measured Spectrix $R_{rs}(\lambda)$ curves.

modeled curves. It can be seen that they match very well to each other, with the only

exception between 660-740nm, where measured $R_{rs}(\lambda)$ are always higher than modeled. This is because chlorophyll fluorescence is not included in the SA $R_{rs}(\lambda)$ model.

Relationships between measured and model-derived absorption and backscattering values are shown in Figure 9. Type 2 linear regression and root-mean-

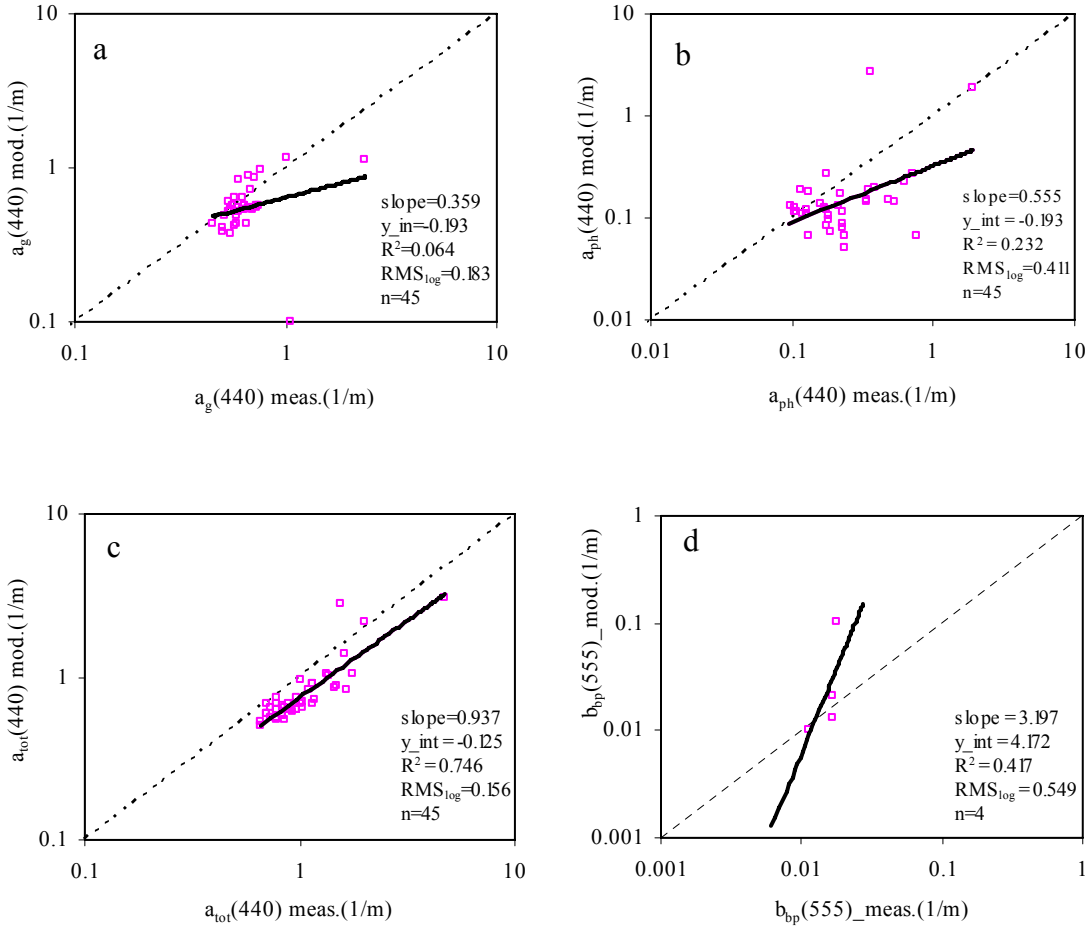

Figure 9. Optimization-derived a) $a_g(440$, b) $a_{ph}(440)$, c) $a_{total}(440)$, d) $b_{bp}(555)$ values obtained from Spectrix $R_{rs}(\lambda)$ data compared to measured values. Original model parameters [*Lee et al.*, 1999] were used. One-to-one lines (dash line) are shown along with type 2 linear regression functions (thick solid) calculated on log-transformed data.

square errors calculated on log-transformed data are shown in Table 3. Total,

Table 3. Statistical results obtained comparing measured versus modeled absorption and backscattering coefficients for Bayboro Harbor (5/2004 ~ 7/2005). Model values were retrieved using the Lee et al. [1998, 1999] optimization technique with original and newly improved model parameters applied to Spectrix $R_{rs}(\lambda)$ data. Type 2 linear regression and RMSE values were calculated from log-transformed data.

	N	Slope	Offset	R^2	$RMSE_{log10}$
$a_g(440)$_orig	45	0.359	-0.193	0.064	0.183
$a_g(440)$_new	45	1.056	-0.066	0.559	0.136
$a_{ph}(440)$_orig	45	0.555	-0.488	0.232	0.411
$a_{ph}(440)$_new	45	0.625	-0.225	0.503	0.222
$a_{tot}(440)$_orig	45	0.937	-0.125	0.746	0.156
$a_{tot}(440)$_new	45	0.87	-0.097	0.809	0.123
$b_{bp}(555)$_orig	4	3.197	4.172	0.417	0.549
$b_{bp}(555)$_new	4	0.818	-0.369	0.377	0.131

phytoplankton and gelbstoff absorption values are typically underestimated as seen by negative y-intercepts. $a_{tot}(440)$ is modeled more accurately (i.e. lower $RMSE_{log10}$) than $a_{ph}(440)$ and $a_g(440)$, because it includes the water absorption, resulting in a larger dynamic range. Measured $a_g(440)$ values are from 0.99 to 6.14 times higher than $a_{ph}(440)$ values, with an average ratio of 3.25 for $a_g(440)$ to $a_{ph}(440)$. This is very typical for a Case 2 harbor, and explains why $a_g(440)$ values are modeled more accurately than $a_{ph}(440)$ values. $a_g(440)$ values exhibit a smaller dynamic range than $a_{ph}(440)$ values (Fig. 9a, b), which may explain the lower R^2 values shown in Table 3. Since only four b_{bp} (555) values are available (Fig. 9d), statistical results are unreliable.

These results indicate that the model parameters derived for the WFS need to be modified to improve optimization derived absorption and backscattering values for Bayboro Harbor.

4.2.2. Modified model parameters for Bayboro Harbor

After careful consideration, it was determined that model parameters for $a_{ph}(\lambda)$ ($A_0(\lambda)$ and $A_1(\lambda)$ from Eq. 15) and $a_g(\lambda)$ (S from Eq. 16) were the most important parameters requiring change when switching study areas from the WFS to Bayboro Harbor. All of the measured $a_{ph}(\lambda)$ spectra were used to generate new $A_0(\lambda)$ and $A_1(\lambda)$ values for Bayboro Harbor. Figure 10 shows an example of how well modeled $a_{ph}(\lambda)$

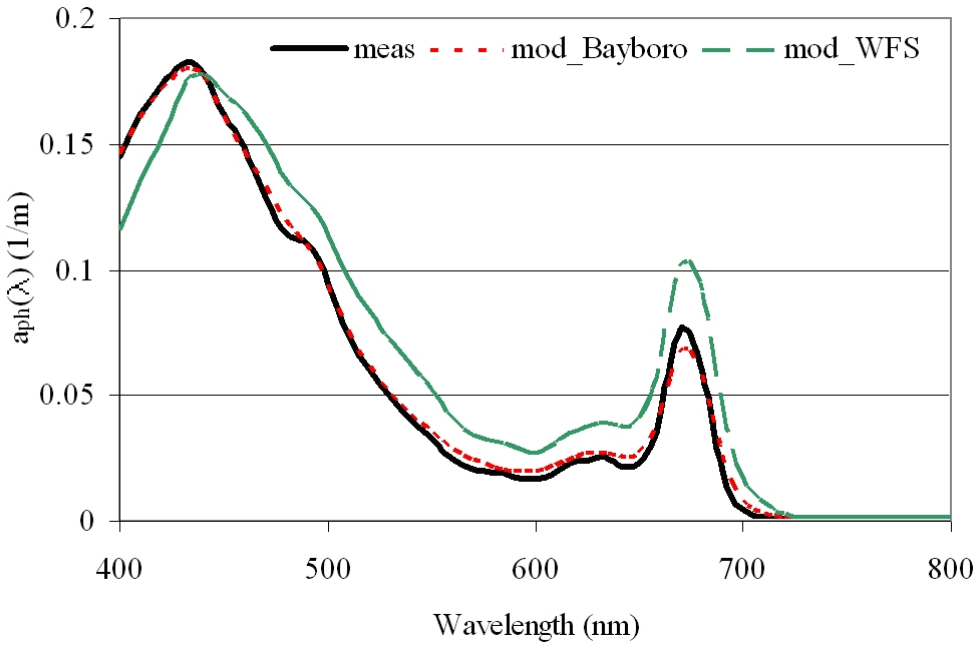

Figure 10. One example of phytoplankton absorption spectra, $a_{ph}(\lambda)$. Thick solid line is $a_{ph}(\lambda)$ measured in Bayboro Harbor, dash line is the modeled $a_{ph}(\lambda)$ derived using the old parameters [*Lee et al.*, 1998], dots line is the modeled $a_{ph}(\lambda)$ derived using the modified A_0, A_1 parameters for Bayboro Harbor.

spectra can match measured $a_{ph}(\lambda)$ with the new parameters, compared to results from using previous Lee et al. [1998] model parameters.

Gelbstoff absorption slopes between 350-500 nm for Bayboro harbor data (May 2004 - July 2005) range from 0.0158 to 0.0185 nm^{-1}, with an average value of 0.0174

nm^{-1} (n=64). An $a_g(\lambda)$ slope of 0.017 nm^{-1} was chosen for the modified parameter set instead of 0.015 nm^{-1}, which was used by the Lee model (1999).

Using these modified $a_{ph}(440)$ and $a_g(440)$ model parameters, the Spectrix $R_{rs}(\lambda)$ data were re-optimized using the Lee et al. [1998, 1999] technique, and an improved set of $a_{tot}(440)$ $a_g(440)$, $a_{ph}(440)$ and $b_{bp}(555)$ values were retrieved (Fig. 11, Table 3).

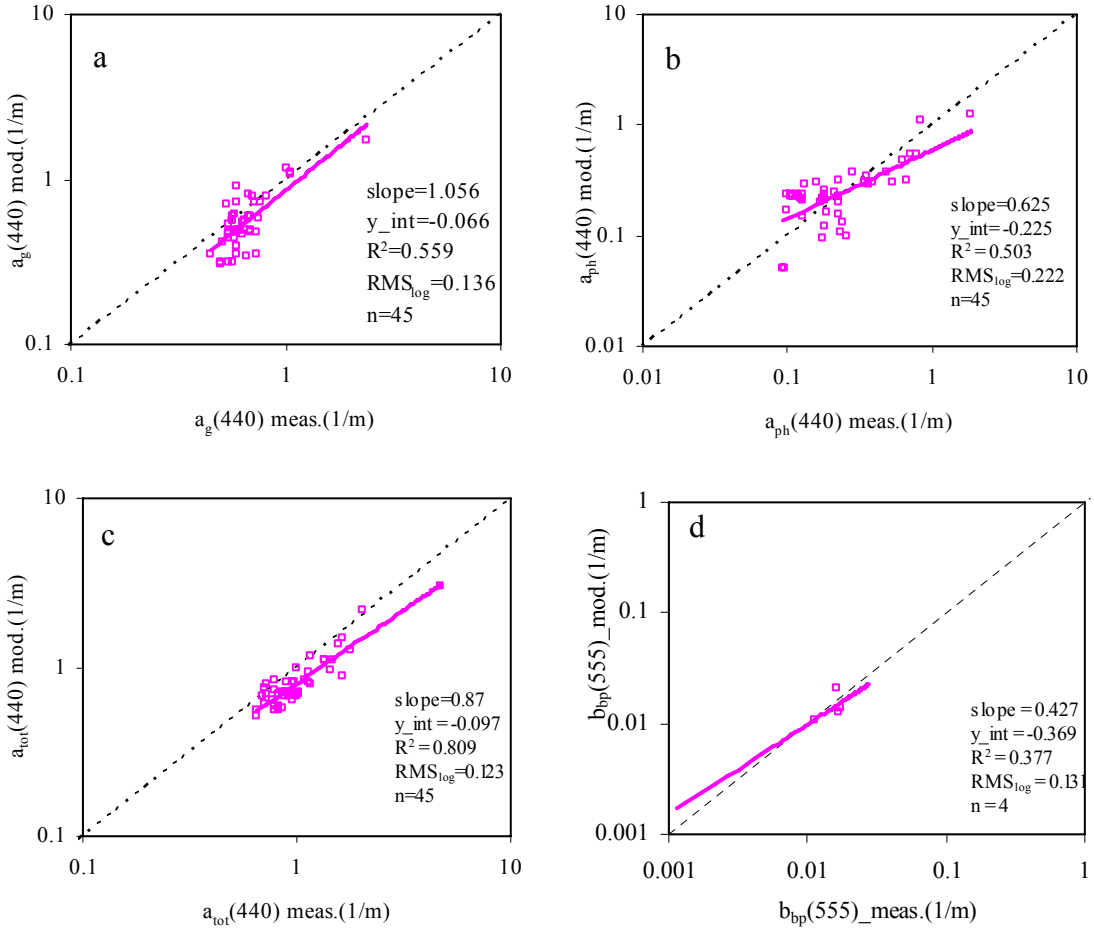

Figure 11. Optimization-derived a) $a_g(440$, b) $a_{ph}(440)$, c) $a_{total}(440)$, d) $b_{bp}(555)$ values obtained from Spectrix $R_{rs}(\lambda)$ data compared to measured values. Model parameters optimized for Bayboro Harbor were used. One-to-one lines (dash line) are shown along with type 2 linear regression functions (thick solid) calculated on long-transformed data

Compared to Figure 9, large improvements both in data point distribution as well as regression trend lines occurred once the parameters were modified. The largest

improvements are in $a_{ph}(440)$ and $b_{bp}(555)$. Notice that modeled $a_g(440)$ and $a_{tot}(440)$ values continue to be somewhat smaller than measured values. The regression results are shown in Table 3 along with $RMSE_{log10}$ estimates. Results show 12% error in $a_{tot}(440)$, 22% error in $a_{ph}(440)$ estimates, 13% error in $a_g(440)$, and 13% error in $b_{bp}(555)$, showing significant improvements over original parameters. The $RMSE_{log10}$ for $a_g(440)$ is almost half of that calculated for $a_{ph}(440)$. This is because gelbstoff dominates the absorption in Bayboro Harbor with an average $a_g(440)$/aph(440) value greater than 3.

4.2.3 Sensitivity analysis

In order to determine why modeled absorption coefficients improved once the model parameters for $a_{ph}(\lambda)$ and $a_g(\lambda)$ were changed, a sensitivity analysis was performed. Spectrix $R_{rs}(\lambda)$ data were re-optimized using slightly different $a_{ph}(\lambda)$ and $a_g(\lambda)$ model parameters than optimal values. Measured versus modeled absorption coefficients were then compared.

Figure 12 shows that changing the gelbstoff slope from 0.017 nm^{-1} to 0.014 nm^{-1} decreases gelbstoff absorption for high $a_g(440)$ values and increases absorption for low $a_g(440)$ values. The opposite is true when a higher a_g slope (0.020 nm^{-1}) is used. The effects on $a_{ph}(440)$ are similar. A lower a_g slope (0.014) causes lower $a_{ph}(440)$ values to decrease and higher values to increase. Detailed error estimates and regression results are shown in Table 4. Overall, deviations in gelbstoff slopes from 0.017 typically lead to increased errors. The only exception is when an a_g slope of 0.014 is used. The $RMSE_{log10}$ for $a_g(440)$ values decreases slightly. However, regression statistics using this slope are worse and $a_{ph}(440)$ values are modeled far less accuratedly ($RMSE_{log10}$ = 0.365).

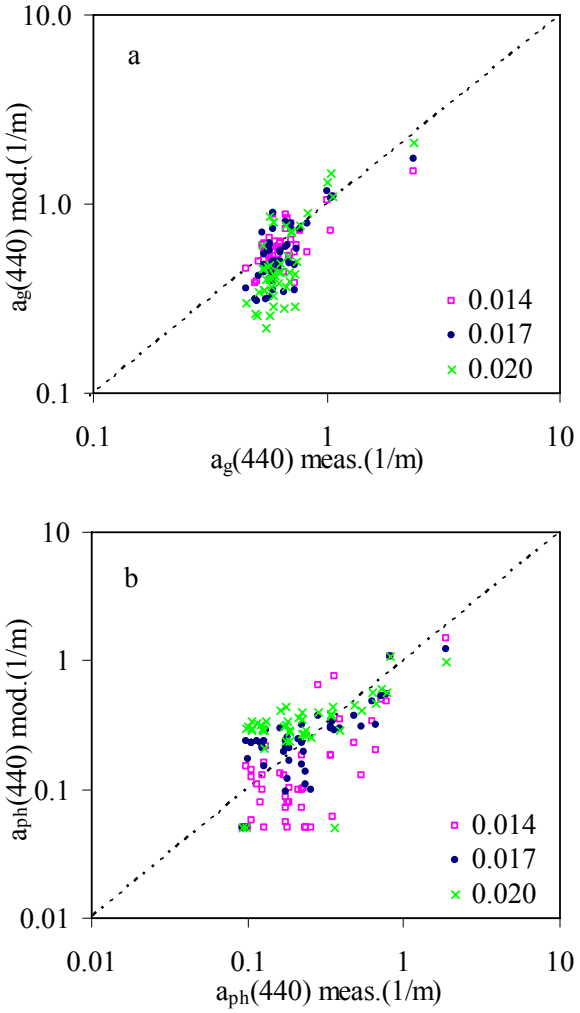

Figure 12. Sensitivity test results showing effects of changing a_g slopes on model outputs for a) $a_g(440)$ and b) $a_{ph}(440)$. Gelbstoff slopes examined were 0.014, 0.017 and 0.020 nm^{-1}. One-to-one lines are shown.

Table 4. Sensitivity test regression results. (a_g slope 0.014,0.017,0.020)

		N	Slope	Offset	R^2	$RMSE_{log10}$
$a_g(440)$	0.014	45	0.748	-0.088	0.516	0.100
	0.017	45	1.056	-0.066	0.559	0.136
	0.020	45	1.374	-0.058	0.564	0.196
$a_{ph}(440)$	0.014	45	0.894	-0.303	0.500	0.365
	0.017	45	0.625	-0.225	0.503	0.222
	0.020	45	0.469	-0.208	0.304	0.297

A similar sensitivity analysis was performed adjusting phytoplankton absorption model parameters $A_0(\lambda)$ and $A_1(\lambda)$ from Eq. 15. New $A_0(\lambda)$ and $A_1(\lambda)$ values generated from Bayboro Harbor $a_{ph}(\lambda)$ sample data (marked AMOS) were compared to the original $A_0(\lambda)$ and $A_1(\lambda)$ values derived from the WFS [*Lee et al.*, 1998]. The results are shown in Figure 13 and Table 5 and indicate that using model $a_{ph}(\lambda)$ parameters developed from

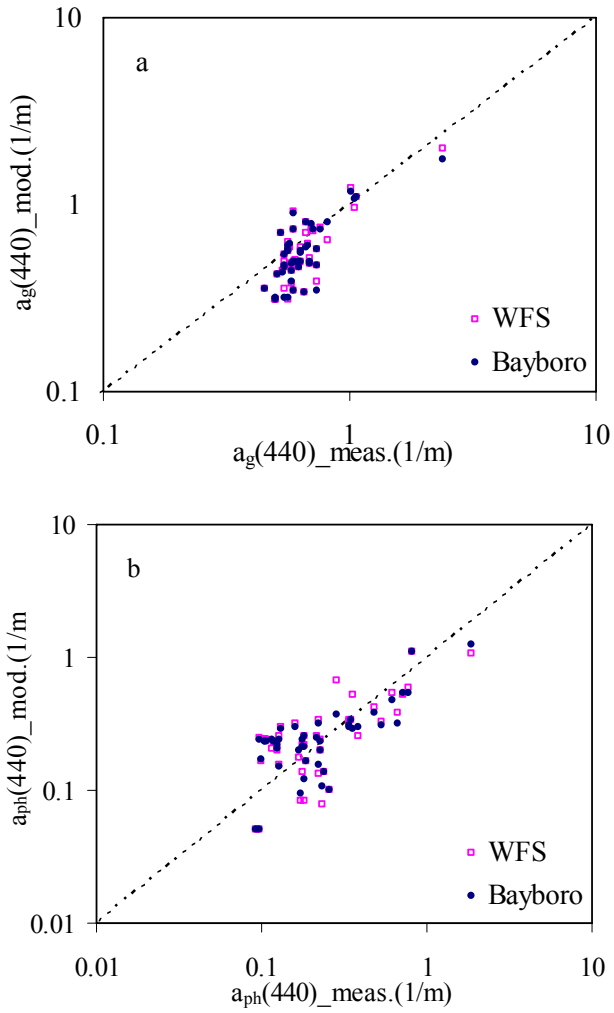

Figure 13. Sensitivity test results showing effects of changing $A_0(\lambda)$ and $A_1(\lambda)$ parameters on model outputs for a) $a_g(440)$ and b) $a_{ph}(440)$. Phytoplankton absorption parameters from Lee et al. [1998] for the West Florida Shelf (WFS) and from Bayboro Harbor data (AMOS) collected during this study are compared. One-to-one lines are shown.

Table 5. Sensitivity test regression results. (A_0A_1_WFS versus A_0A_1_Bayboro)

		N	Slope	Offset	R^2	$RMSE_{log10}$
$a_g(440)$	WFS	45	1.081	-0.057	0.583	0.132
	Bayboro	45	1.056	-0.066	0.559	0.136
$a_{ph}(440)$	WFS	45	0.662	-0.200	0.460	0.243
	Bayboro	45	0.625	-0.225	0.503	0.222

Bayboro Harbor data causes the error in $a_{ph}(440)$ to decrease slightly (from 24% to 22%). No significant deviations in $a_g(440)$ estimates were observed due to changes in $A_0(\lambda)$ and $A_1(\lambda)$ values.

The sensitivity tests performed indicate that changing gelbstoff slopes affect model outcomes more so than changing the $a_{ph}(\lambda)$ parameters. This makes sense since gelbstoff dominates the absorption values in Bayboro Harbor with average $a_g(440)/a_{ph}(440)$ values greater than three.

4.3 Validation of AMOS $R_{rs}(\lambda)$ data

Beginning in May of 2004, AMOS was deployed in the Bayboro Harbor (Saint Petersburg, Florida). Automated $R_{rs}(\lambda)$ derived from AMOS measurements for May 2004 (hourly between 15:00 and 19:00 GMT) are shown in Figure 14. Notice that compared to the Spectrix $R_{rs}(\lambda)$ curves (Fig. 7), offsets exist amongst many of these spectra. This may be due to the presence of sun glint and/or removal of too little sky light from the data. Similar to the Spectrix data, reflectance peaks occur at ~570 and 685 nm. Spectra are slightly noisier due to instrument design (fiber optic cable).

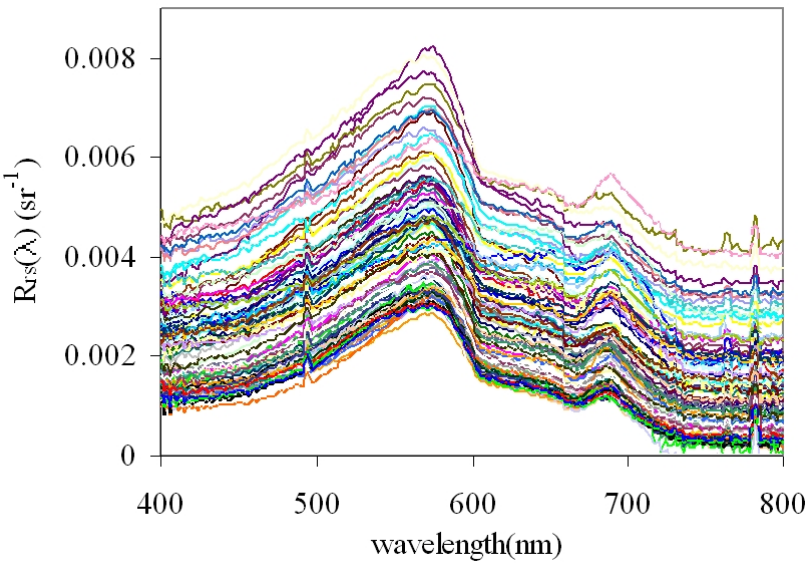

Figure 14. Remote-sensing reflectance spectra from the AMOS sensor, May 2004 (hourly between 15:00 and 19:00 GMT). Measurements were collected in Bayboro Harbor (St. Petersburg, Florida).

A comparison between several AMOS remote-sensing reflectance spectra and $R_{rs}(\lambda)$ collected nearby manually using hand-held Spectrix (within 30 minutes) is shown in Figure 15. Of the 3 stations used to show the variations, the spectra with the highest reflectivity at 570nm provides the closest match between AMOS and Spectrix data. The spectra with the lowest reflectivity at 570nm provides the worst match. All spectra exhibit peak reflectivity ~570nm indicating consistent spectral calibrations for both sensors. It can be seen from this figure also that the AMOS sensor consistently exhibits more reflectance at the blue end (~400 nm) compared to the Spectrix sensor.

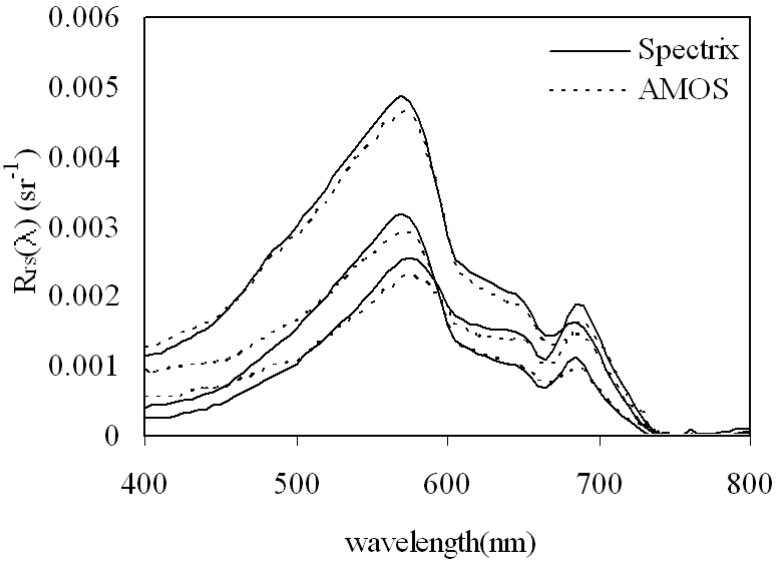

Figure 15. Comparisons between Spectrix and AMOS remote-sensing reflectance spectra measured in Bayboro Harbor (St. Petersburg, Florida) during May 2004.

To quantitatively compare $R_{rs}(\lambda)$ measurements obtained from the AMOS and Spectrix sensors during May 2004, three wavelengths (blue=440nm, green=570nm, and red=640nm) were chosen (Fig. 16). Error estimates obtained from non-log transformed data are listed in Table 6. AMOS $R_{rs}(\lambda)$ underestimates Spectrix values at 570 and 640nm. $RMSE_{lin}$ estimates are only about 13% for both wavelengths. At 440nm, AMOS overestimates Spectrix $R_{rs}(\lambda)$ values ($RMSE_{lin}$ >400%).

Table 6. Regression results between measured $R_{rs}(\lambda)$ by direct Spectrix versus AMOS $R_{rs}(\lambda)$ at 440, 570 and 640nm wavelengths.

		N	Slope	Offset	R^2	$RMSE_{lin}$
440nm	uncorrected	8	0.651	0.0006	0.888	4.647
	corrected	8	0.909	0.0001	0.933	0.438
570nm	uncorrected	8	0.921	-6E-05	0.921	0.129
	corrected	8	0.967	-3E-04	0.903	0.152
640nm	uncorrected	8	0.820	0.0001	0.913	0.126
	corrected	8	0.873	3E-05	0.8773	0.150

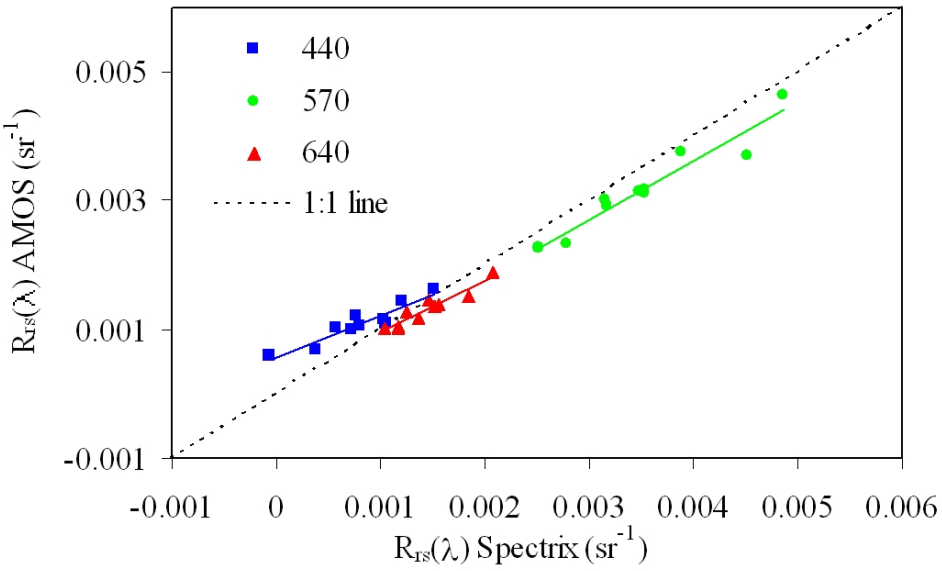

Figure 16. AMOS versus Spectrix remote-sensing reflectance values at 440, 570 and 640nm. Measurements were collected from Bayboro Harbor (St. Petersburg, Florida) in May 2004. Linear best-fit regression lines (solid) are shown along with a one-to-one line (dotted).

If $a_g(440)$ values are to be modeled successfully from $R_{rs}(\lambda)$ data, then accurate blue reflectance values are essential since gelbstoff absorbs blue light strongly (Fig. 4). From Figure 11, recall that $a_g(440)$ values were slightly underestimated when derived from Spectrix $R_{rs}(\lambda)$ data using the Lee et al. [1998, 1999] optimization technique with the model parameters modified for Bayboro Harbor. Given that AMOS blue reflectance values are higher than Spectrix reflectance values (Fig. 16), and $R_{rs}(\lambda)$ is inversely proportional to $a(\lambda)$ (Eq. 7), AMOS modeled $a_g(440)$ values would underestimate measured $a_g(440)$ values even more than Spectrix modeled $a_g(440)$ values.

In order to retrieve accurate $a_g(440)$ values from the AMOS $R_{rs}(\lambda)$ data, this excess blue light must first be removed. Looking back at the actual design of the AMOS and Spectrix radiometers, one large difference is the field-of-view (FOV) whereby the

AMOS sensor has an FOV of ~25^{o} while the Spectrix has one of only ~10^{o}. Taking this into consideration, perhaps not enough skylight was subtracted from the upwelled radiance spectra due to wave facets bringing in light reflected from much larger angles, causing the blue reflectance values to be too high. In order to solve this problem, an effective "Rayleigh-like" correction term was added to the optimization technique to remove excess blue light from the AMOS $R_{rs}(\lambda)$ data. This term, $Ray(\lambda) = Ray(400)(400/\lambda)^{4.1}$ is subtracted from $R_{rs}(\lambda)^{meas}$ in Eq.(19) along with Δ. Ray(400) and Δ are then iteratively optimized along with $a_g(440)$, $a_{ph}(440)$, $b_{bp}(555)$, $\rho(550)$ and H using the Lee et al. [1998] optimization technique (Fig. 17).

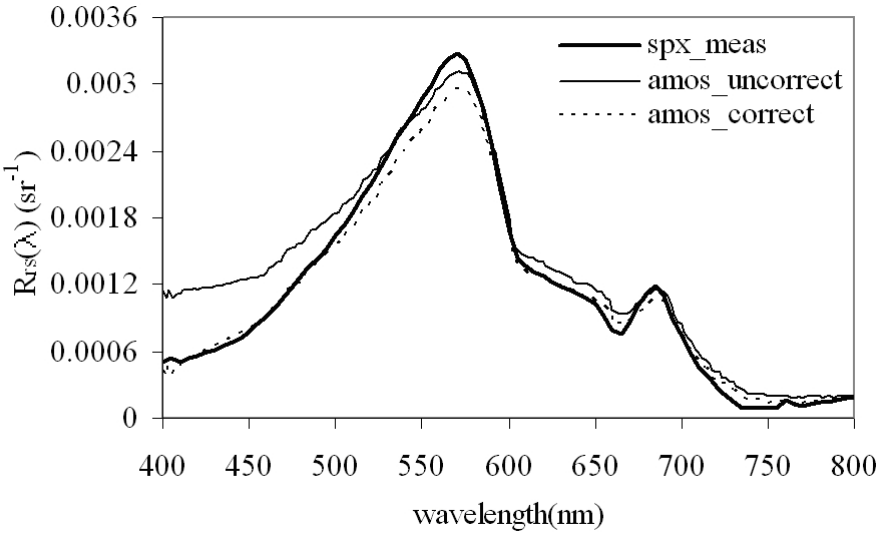

Figure 17. An example of remote-sensing reflectance spectra obtained by the AMOS and Spectrix sensors from Bayboro Harbor (St. Petersburg, Florida) on May 6, 2004. Excess blue light is removed from the AMOS $R_{rs}(\lambda)$ using an effective "Rayleigh-like" correction term incorporated into the Lee et al. [1999] optimization model.

Corrected AMOS $R_{rs}(\lambda)$ data are then compared to the Spectrix $R_{rs}(\lambda)$ data again, and results are shown in Figure 18. AMOS $R_{rs}(\lambda)$ decreased at the blue end (440nm), matching the one-to-one line when compared to the Spectrix $R_{rs}(\lambda)$. The regression

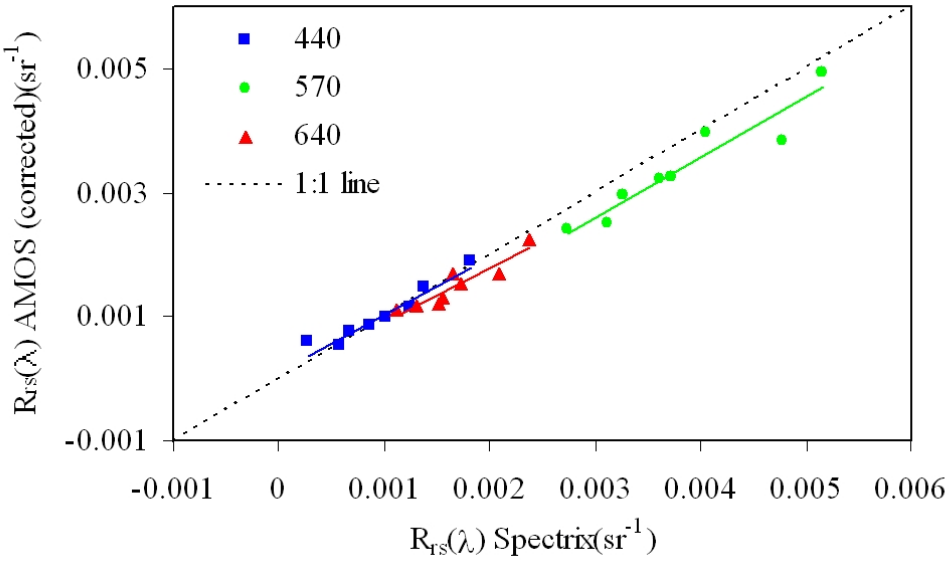

Figure 18. Corrected AMOS versus Spectrix remote-sensing reflectance values at 440, 570 and 640nm obtained from Bayboro Harbor (St. Petersburg, Florida) in May 2004. AMOS $R_{rs}(\lambda)$ data were corrected by incorporating an effective "Rayleigh-like" correction term into the Lee et al. [1999] optimization model. Linear best-fit regression lines (solid) are shown along with a one-to-one line (dotted).

results show ten-fold improvements in $RMSE_{lin}$ at 440 nm (Table 6), although, green (570nm) and red (640nm) $RMSE_{lin}$ increase slightly. Recall, however, that it is the blue reflectance values that are important for accurate absorption coefficient retrievals.

4.4 AMOS Time-series analysis

Using the modified model parameters discussed in Section 4.2, a time series of $a_g(440)$, $a_{ph}(440)$ and $b_{bp}(555)$ values were derived from "Rayleigh-corrected" AMOS $R_{rs}(\lambda)$ data for May 2004 (Figure 19). Directly measured values are also plotted for validation purposes.

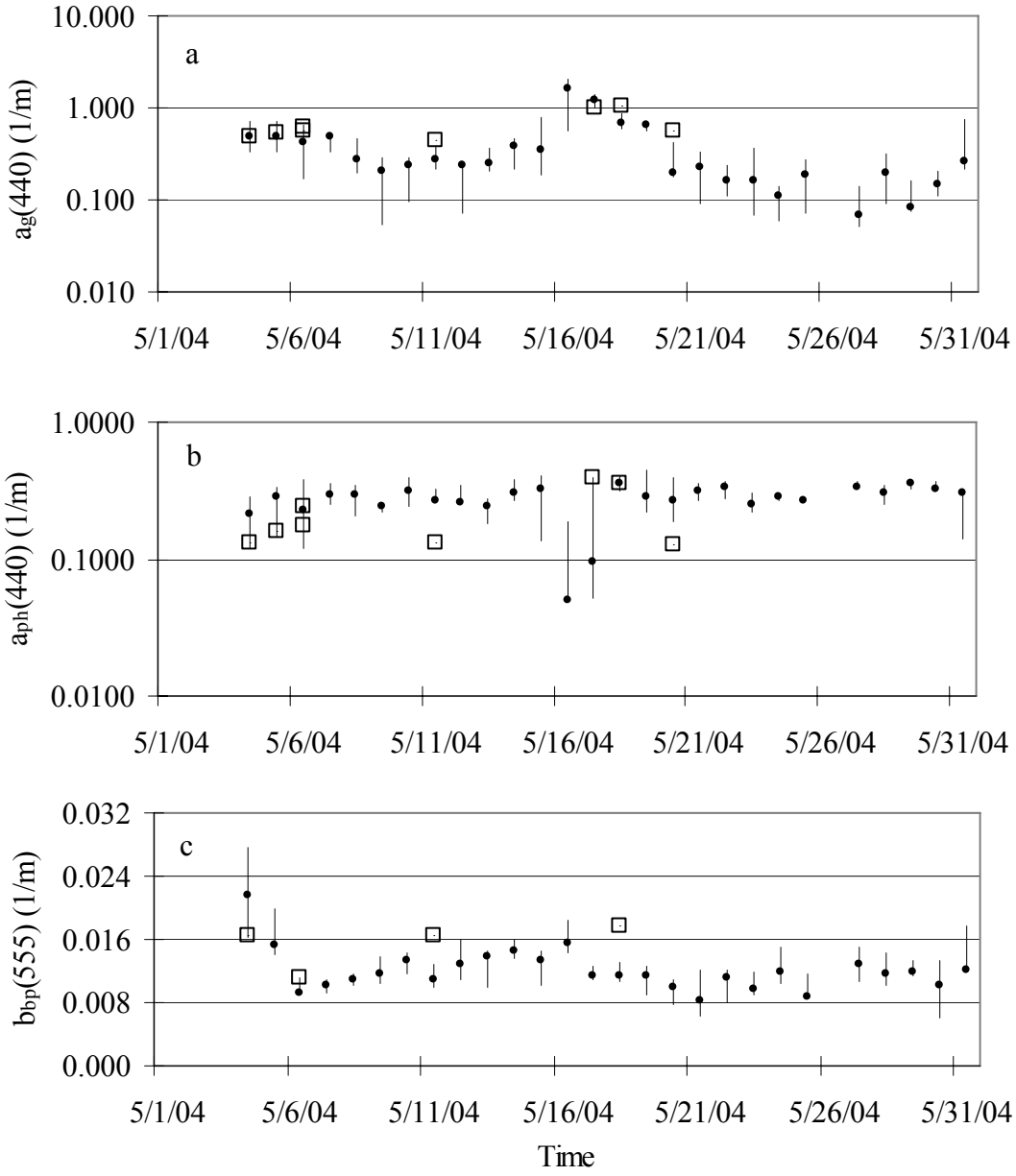

Figure 19. AMOS $R_{rs}(\lambda)$ derived a) $a_g(440)$, b) $a_{ph}(440)$, c) $b_{bp}(555)$ values for Bayboro Harbor (St. Petersburg, FL) May 2004. Values were derived using the Lee et al. [1999] optimization model modified for Bayboro Harbor. The boxes are measured values.

Modeled $b_{bp}(555)$ values derived from AMOS $R_{rs}(\lambda)$ data compare well with measured values exhibiting only a slightly higher $RMSE_{log10}$ (19%) compared to when

Spectrix derived values are used ($RMSE_{log10}$ = 13%) (Fig. 20c, Table 7). Retrieved values for gelbstoff and phytoplankton absorption show a similar pattern with Spectrix $R_{rs}(\lambda)$ retrieved values outperforming the AMOS $R_{rs}(\lambda)$ retrieved values, but with much larger $RMSE_{log10}$ (Fig. 20a,b, Table 7). AMOS retrieved $a_g(440)$ values may be underestimated

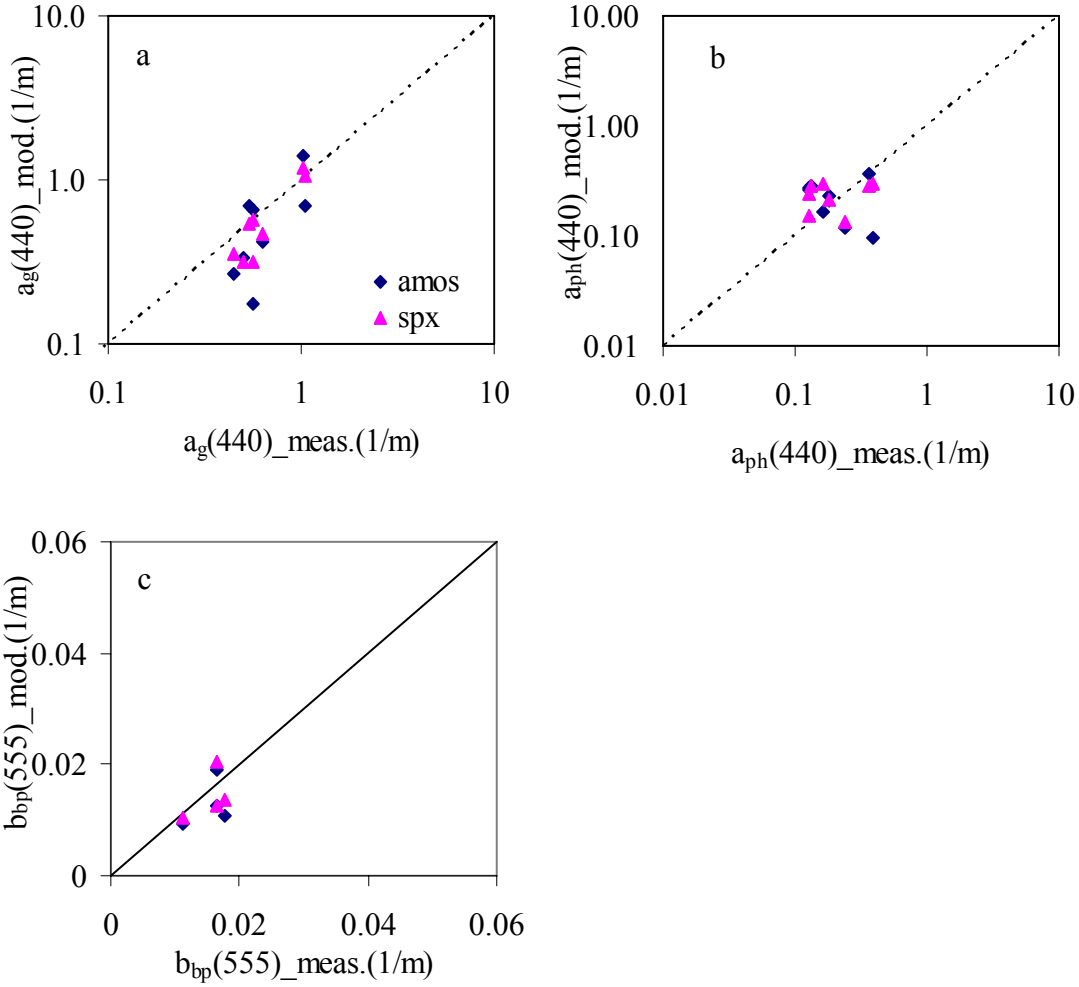

Figure 20. Measured values compared to optimization model outputs. a) $a_g(440)$; b) $a_{ph}(440)$; c) $b_{bp}(555)$.

Table 7. Regression results between AMOS and Spectrix $R_{rs}(\lambda)$ modeled and measured values of $a_{ph}(440)$, $a_g(440)$, $b_{bp}(555)$. Error estimates $RMSE_{log10}$ are consistent with those of Carder et al. (2004), although the other statistics are worse.

	N	Slope	Offset	R^2	$RMSE_{log10}$
$a_g(440)$_amos	8	1.422	-0.036	0.466	0.271
$a_g(440)$_spx	8	1.484	0.017	0.836	0.151
$a_{ph}(440)$_amos	8	-0.421	-0.987	0.171	0.363
$a_{ph}(440)$_spx	8	0.160	-0.527	0.053	0.244
$b_{bp}(555)$_amos	4	0.824	-0.406	0.301	0.187
$b_{bp}(555)$_spx	4	0.818	-0.369	0.377	0.131

due to inadequate sky light removal, even after spectra were corrected using the effective "Rayleigh-like" term. Modeled $a_{ph}(440)$ values are typically underestimated especially when $a_g(440)$: $a_{ph}(440)$ values are high (Figure 20b).

Chlorophyll concentrations can be retrieved accurately from measurements of $a_{ph}(440)$ if the relationship between them is known [*Bricaud et al.*, 1995]. Measured $a_{ph}(440)$ data in this study for May 2004 show a strong, positive correlation with chlorophyll concentration ($R^2 = 0.964$, n = 8) (Fig. 21a). Since modeled $a_{ph}(440)$ values

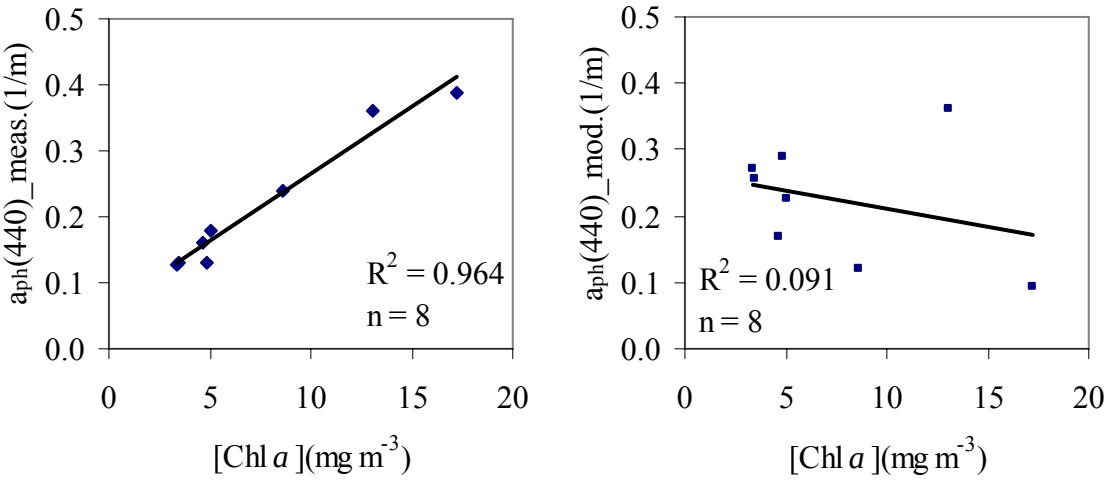

Figure 21. Measured chlorophyll a concentration from Bayboro Harbor compared to: a) measured $a_{ph}(440)$; b) modeled $a_{ph}(440)$.

are highly inaccurate exhibiting an $RMSE_{log10}$ of 36% (Fig. 20b), a weak negative correlation with chlorophyll concentration is observed ($R^2 = 0.09$, n = 8) (Fig. 21b). This indicates that $a_{ph}(440)$ data modeled from AMOS $R_{rs}(\lambda)$ data cannot be used to monitor chlorophyll concentrations. Therefore, an alternative approach for deriving chlorophyll concentrations from AMOS $R_{rs}(\lambda)$ data is needed instead.

It has been shown that the height of the chlorophyll fluorescence peak (~685nm) above background radiances is highly correlated with the chlorophyll concentrations [*Letelier and Abbott*, 1996] suggesting that such fluorescence line heights (FLH) (Fig. 22) may be used to obtain estimates of chlorophyll concentrations from $R_{rs}(\lambda)$. In this study FLH is defined as

$$FLH = R_{rs}(690) - (R_{rs}(670) - \frac{(R_{rs}(670) - R_{rs}(750)) * (690 - 670)}{750 - 670}) \qquad (20).$$

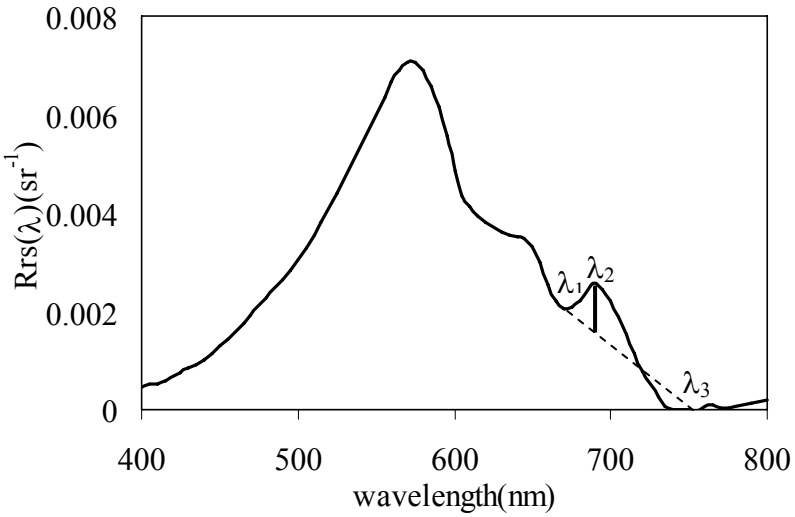

Figure 22. Fluorescence line heights (FLH). Height above an imaginary line between 670 and 750nm. λ_1=670nm, λ_2=690nm, λ_3=750nm.

Chlorophyll concentrations in this study are more highly correlated with FLH's calculated from AMOS $R_{rs}(\lambda)$ data ($R^2 = 0.692$, n = 11) (Fig. 23) than with modeled

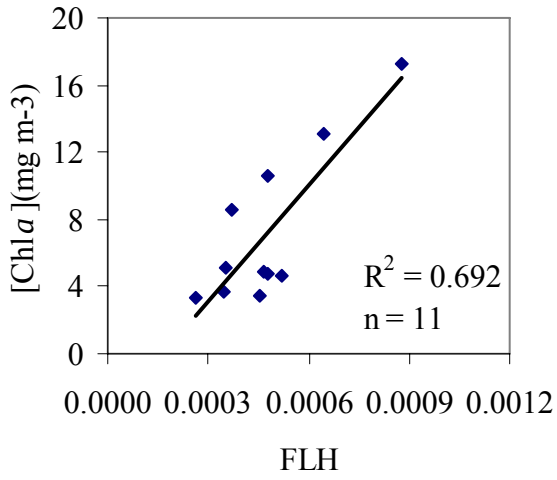

Figure 23. Measured chlorophyll *a* concentration from Bayboro Harbor compared to FLH.

$a_{ph}(440)$ data (Fig. 21b). Applying the best-fit linear relationship derived between AMOS FLH's and measured chlorophyll concentrations to AMOS $R_{rs}(\lambda)$ data for May 2004 results in the time series shown in Figure 24. The time series from AMOS provided interpolations for chlorophyll values between measurements.

Meteorological conditions and tide information are shown in Figure 24. Many interesting features in model-derived $a_g(440)$, $b_{bp}(555)$ and [Chl *a*] (Figs. 19, 24) match nicely with these environmental forcings. The higher wind values on May 4th coincide with higher $b_{bp}(555)$ values, while chlorophyll concentrations stayed low. This is likely the result of bottom sediment re-suspension caused by the wind. Precipitation (Fig. 25a) shows about 1 inch of rainfall on May 3rd which could also contribute to increased nutrients along with nutrients released by erosion. These may be responsible for the

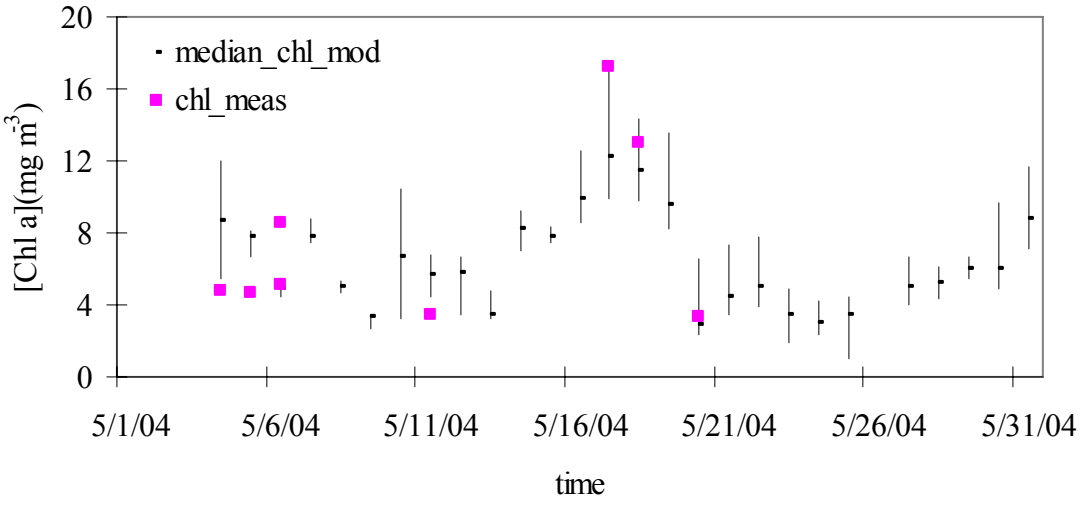

Figure 24. Chlorophyll *a* concentrations using FLH method (marked circles) derived by AMOS $R_{rs}(\lambda)$ data for May 2004 at Bayboro Harbor. Directly measured chlorophyll *a* concentrations are marked with squares.

increase of chlorophyll concentration from May 4th to May 7th. The small peak in $a_g(440)$ during this time could be the result of runoff of gelbstoff. Higher $b_{bp}(555)$ from May 12th to 18th also match the wind speed information during this period.

The large amount of rainfall on May 15th (Fig. 25a) is probably responsible for the steady [Chl *a*] increase until May 19th when nutrients were brought in from runoff as well as re-suspension, also indicated by higher $b_{bp}(555)$ values. Note the prominent peak shown in $a_g(440)$ from May 17 to 19 (Fig. 19) indicative of increased runoff.

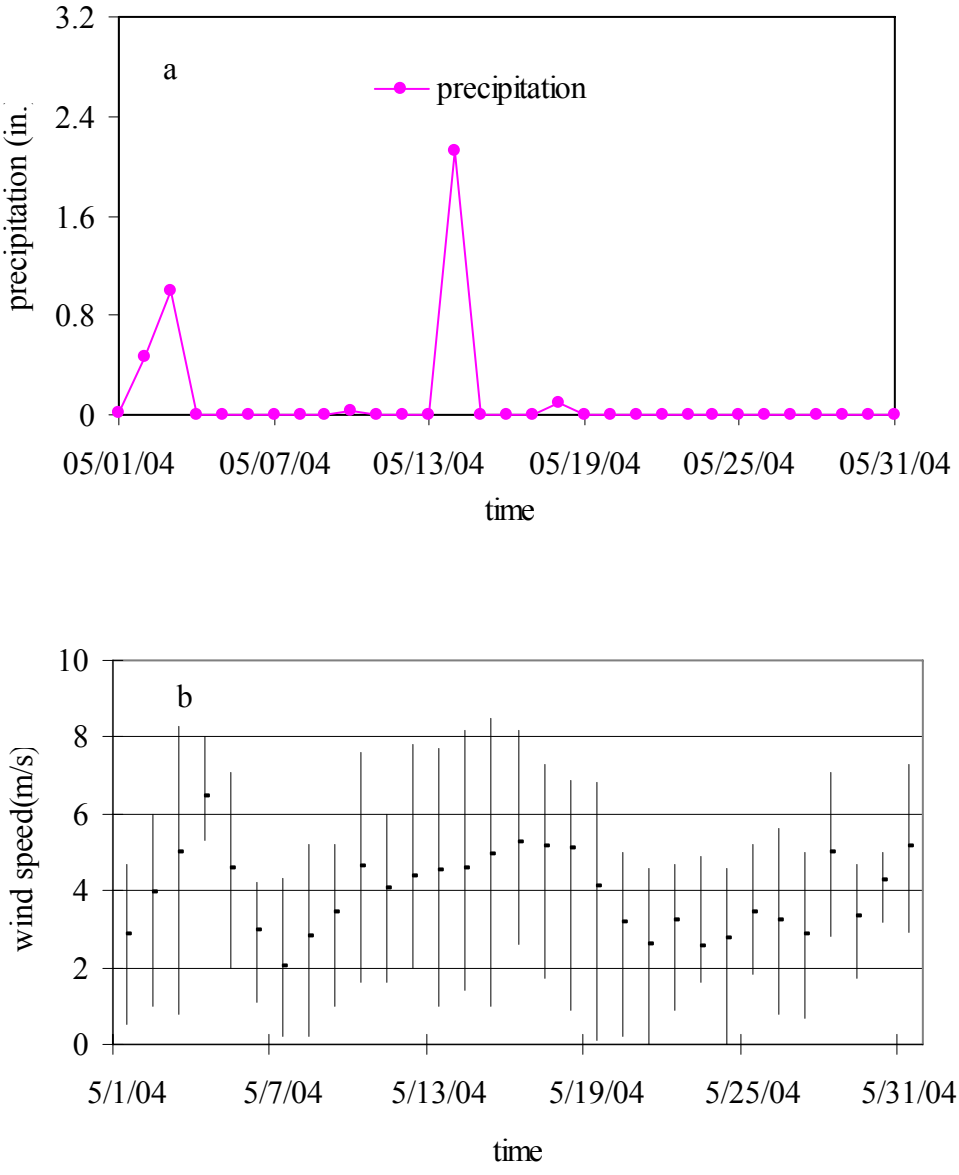

Figure 25. Meteorological parameters of May 2004 near study area. a) rainfall data (from National Weather Service at Saint Petersburg Station; b) hourly wind speed from buoy located on West Florida Shelf. Bar height represents wind speed range, with middle dots represent the average daily wind speed (b from NOAA CO-OPS website, for St. Petersburg, Florida location).

Data from AMOS underwater units collected during mid-May further validate the pattern observed for the AMOS $R_{rs}(\lambda)$ derived data (Fig. 26). Measured *in situ*

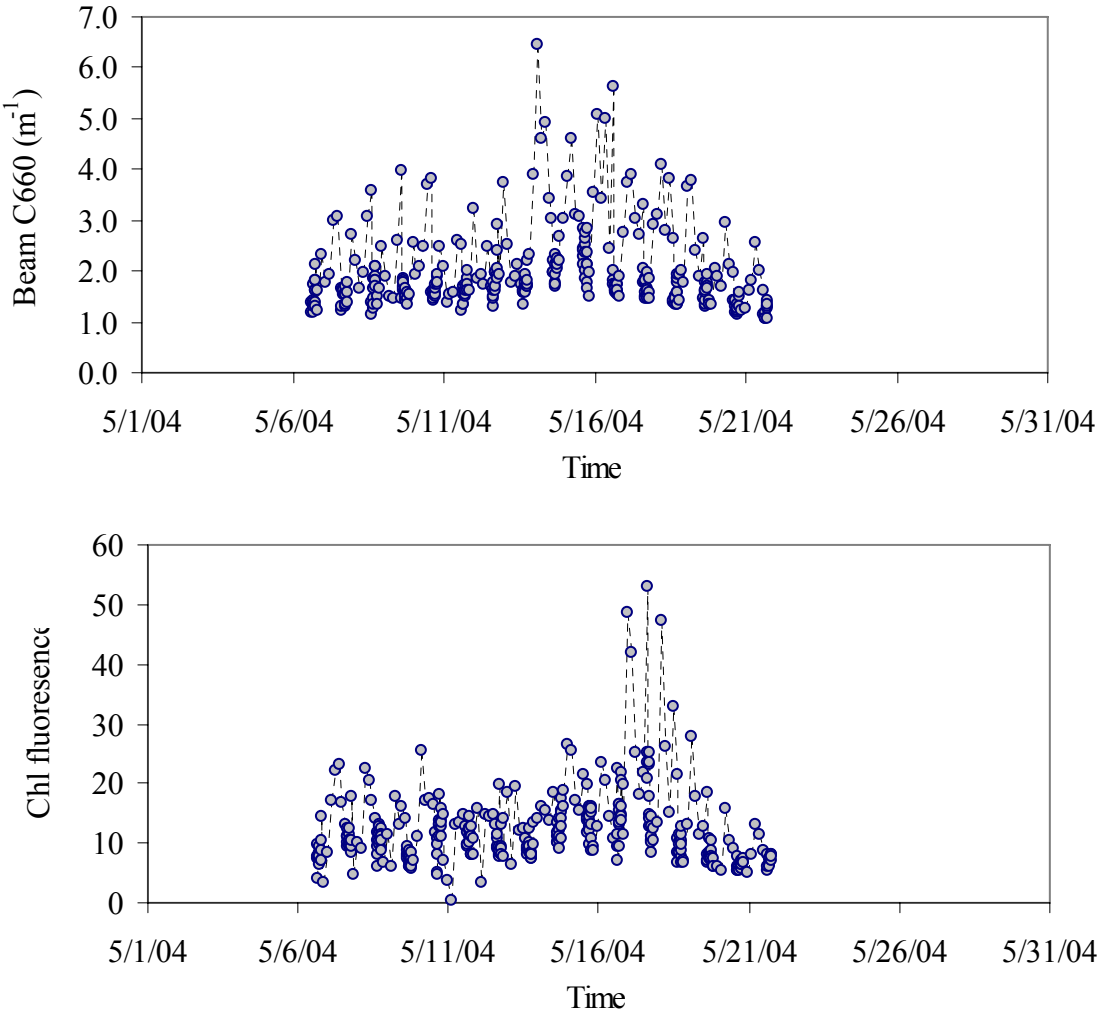

Figure 26. AMOS underwater instrument measurements from May 7 to May 21 at Bayboro Harbor: a) beam-c (660nm); b) uncalibrated chlorophyll fluorescence by fluorometer.

chlorophyll fluorescence values match nicely with the chlorophyll *a* concentrations calculated by the FLH-method (Fig. 24), especially for the peak values from May 17 to 19. The transmissometer-measured beam c(660) values show peak values around May 15-18 (Fig. 26a). This elevated change is much higher than what the modeled $b_{bp}(555)$ values indicate (Fig. 19c).

These pattern co-variations can also be seen towards the end of May, when chlorophyll concentrations become lower along with lower wind speed and lack of rainfall. Brief periods of stronger winds did occur at the end of May, but the directions were mostly from north and did not affect our research area significantly.

5. DISCUSSION

From May 2004 to July 2005 when AMOS was deployed in Bayboro harbor, significant variability in optical properties was observed. Measured chlorophyll *a* concentrations ranged from 2.5 to 47.7 mg m^{-3}, $a_{ph}(440)$ ranged from 0.1 to 1.9m^{-1}, and $a_g(440)$ ranged from 0.5 to 2.4 m^{-1}. In order to derive absorption and backscattering coefficients and chlorophyll concentrations accurately from above-water remote-sensing reflectance spectra for such Case 2 waters, accurate $R_{rs}(\lambda)$ data and a successful $R_{rs}(\lambda)$ inversion technique are required.

Prior to using the AMOS $R_{rs}(\lambda)$ data to derive a time-series of IOP's and chlorophyll concentrations, however, it was necessary for this data first to be validated. Reflectance data measured using a hand-held Spectrix radiometer was used for this purpose. Higher $R_{rs}(\lambda)$ values at 440nm measured by AMOS compared to those measured by the Spectrix sensor indicated that perhaps not enough skylight had been removed from the AMOS upwelled radiance data. While both sensors viewed the water and sky at 30^o from nadir and zenith, respectively, the larger field-of-view for AMOS (25^o) compared to the Spectrix (10^o) sensor, necessitates the use of a higher Fresnel reflectance factor with the AMOS data to be removed excess skylight [*Mobley*, 1994].

Instead of reprocessing the AMOS $R_{rs}(\lambda)$ data using a higher Fresnel factor, an effective "Rayleigh-like" correction factor was included in the Lee et al. [1999]

optimization model to allow variable amounts of excess blue-rich light to be removed. This correction term forced the AMOS and Spectrix $R_{rs}(440)$ data to agree more closely. These improvements are very important, since the main focus of this study which is to obtain accurate $a_{ph}(440)$ and $a_g(440)$ estimates requires a good understanding of the blue part of the spectrum. Differences in green ($R_{rs}(570)$) and red ($R_{rs}(640)$) reflectance values, however, remained high, and can be attributed to other sources.

Spatial and temporal sampling differences must be considered when comparing $R_{rs}(\lambda)$ values from the AMOS and Spectrix sensors. Bi-directional reflection due to varying viewing angles may introduce differences in $R_{rs}(\lambda)$ when surfaces are not Lambertian. Since the Spectrix and AMOS sensors do not look at the same spot in the sky or water at sampling time, on top of viewing solid-angle differences, perfect matches should not be expected when $R_{rs}(\lambda)$ curves from both sensors are compared side-by-side. What's more, since Spectrix measurements were made closer to the seawall compared to AMOS measurements, differences in water depth could also cause mismatches, especially in the green transparency window.

Timing differences between the instrument measurements may also explain the small differences observed in $R_{rs}(\lambda)$ between the AMOS and Spectrix sensors. Even though Spectrix measurements were made within 30 minutes of AMOS mesurements, solar radiance inputs due to cloudiness and water conditions (wind riffles) can change by the second to introduce differences, especially when considering harbor areas with shallow bottoms.

Compared to waters of the west Florida shelf, Bayboro Harbor is a highly gelbstoff-dominated environment. Ratios of $a_g(440)$-to- $a_{ph}(440)$ ranged from 1.0 to 6.7

during this study period with an average value of 3.3, which is highly indicative of a Case 2 water environment. Relative to the total absorption coefficient at 440nm, $a_{ph}(440)$ and $a_g(440)$ contributed 24% and 65% to $a_{tot}(440)$, respectively, on average. As a result, the Lee et al. [1999] optimization model had to be modified to perform successfully in Bayboro Harbor.

Changes made to the $a_{ph}(\lambda)$ and $a_g(\lambda)$ parameters in the semi-analytic model to more accurately represent the measured Bayboro Harbor data improved IOP estimates derived from Spectrix $R_{rs}(\lambda)$ data. Compared to when the original Lee et al. [1999] parameters were used, root-mean-square errors generated between log-transformed measured versus modeled $a_{ph}(440)$ data decreased from 41% to 22%. Similarly, errors for $a_g(440)$ decreased from 18% to 14% and errors for $b_{bp}(555)$ decreased from 55% to 13%. Retrievals for $a_g(440)$ were much more accurate compared to those for $a_{ph}(440)$, again since Bayboro harbor is gelbstoff-dominated. Modeled values for $a_g(440)$ were slightly underestimated perhaps because bottom contributions which cause higher green reflectivity were overestimated. Modeled bottom depths were typically much lower than the true depth supporting this theory.

In order to put the retrieved errors calculated in this study for $a_{ph}(440)$ and $a_g(440)$ into perspective, results are compared to errors calculated semi-analytically for a large global data set (n = 656) using only SeaWiFS wavebands (412, 443, 490, 510, and 555nm) [*Carder et al.*, accepted]. This global data set was made available by the International Ocean Colour Coordinating Group (IOCCG) for an algorithm testing round robin and contained no bottom effects. Compared to IOCCG results, $a_{ph}(440)$ values were

modeled slightly more accurately for the IOCCG data set ($RMSE_{log10}$ = 19.5%) and $a_g(440)$ values were modeled much less accurately ($RMSE_{log10}$ = 27.9%).

Since model retrievals for $a_{ph}(440)$ were not very accurate for this study owing to the gelbstoff-dominated nature of Bayboro Harbor, chlorophyll concentrations were derived from AMOS $R_{rs}(\lambda)$ data using fluorescence line heights. While the algorithm developed in this study may be highly season-specific (i.e. will only work with AMOS data), site-specific, and time-specific (i.e. other relationships may be observed for different sensors), chlorophyll concentrations were derived fairly accurately ($RMSE_{log10}$ = 21.5%) using only three $R_{rs}(\lambda)$ wavebands (670, 690, 750nm). Results from deriving and testing numerous empirical band-ratio algorithms that require SeaWiFS wavebands on a large global dataset (n = 919) show similar errors with $RMSE_{log10}$ values ranging from 17.2 to 31.1% [*O'Reilly et al.*, 1998].

A recent NASA report on ocean color and carbon for the Chesapeake Bay (Case 2) [*Signorini et al.*, 2005] shows that the best statistical results obtained for modeled chlorophyll concentrations using the regionally tuned Garver-Siegel-Maritorena (GSM01_CB) semi-analytic algorithm [*Maritorena et al.*, 2002] yield an absolute percent difference (APD) equal to 68.34%. This SA algorithm requires $R_{rs}(\lambda)$ data at SeaWiFS wavebands. Chlorophyll concentrations derived from AMOS $R_{rs}(\lambda)$ FLH data for May 2004 in Bayboro Harbor were estimated more accurately (APD = 41.26%) compared to the GSM01-CB results.

6. CONCLUSIONS

The measured high levels of chlorophyll concentrations in Bayboro Harbor indicate that it is a highly productive area. Using the original parameters for the Lee et al. [1999] SA model to retrieve in-water optical properties ($a_{ph}(440)$, $a_g(440)$ and $b_{bp}(555)$), results in large retrieval errors. New optimization model parameters were applied, and retrieval results show much improvement supporting the hypothesis that the Lee et al. [1998, 1999] semi-analytical hyperspectral remote-sensing model could be fitted to work in very turbid Bayboro Harbor water. A sensitivity analysis further demonstrated the effectiveness of the new parameters.

AMOS $R_{rs}(\lambda)$ data from May 2004 were used to evaluate the system performance against in-situ measurements by the hand-held Spectrix sensor. The traditional approach to derive measured $R_{rs}(\lambda)$ spectra does not work well with AMOS. A new approach is used to calculate AMOS $R_{rs}(\lambda)$ from measured downwelling irradiance and upwelling radiance, with the removal of proper Raleigh scattering and model residual (Δ) at 750nm. The results show significant improvements in the blue part of the spectrum, which enables better model estimates.

The SA model derived time-series values for the month of May 2004, namely $a_g(440)$ and $b_{bp}(555)$, correspond nicely to measured values as well as to external environmental changes. Because of the dominance of absorption by gelbstoff, modeled

$a_{ph}(440)$ values cannot be used to accurately estimate chlorophyll a concentrations. However, improved estimates of chlorophyll concentration in these turbid waters were obtained from fluorescence line heights. This validates the effectiveness of AMOS as a tool not only to provide measurements for high-altitude sensor-calibration purposes, but also to generate time series for coastal marine ecosystems.

The optimization model used demonstrated slightly biased errors for this specific location and model parameters. This might need to be fine-tuned for optimal results. Better results could also arise from better AMOS instrument calibration and its situation over a flat bottom away from a seawall. The success of AMOS results encourages further testing and implementation of such automated, continuous data sampling stations for wide-area field deployment.

LIST OF REFERENCES

Austin, R.W., and T.J. Petzold, The determination of the diffuse attenuation coefficient of sea water using the coastal zone color scanner, in *Oceanography from Space*, edited by J.F.R. Gower, pp. 239-256, Plenum Press, New York, 1981.

Bidigare, R.R., J.H. Morrow, and D.A. Kiefer, Derivative analysis of spectral absorption by photosynthetic pigments in the western Sargasso Sea, *Journal of Marine Research*, *47*, 323-341, 1989.

Bricaud, A., M. Babin, and A. Morel, Variability in the chlorophyll-specific absorption coefficients of natural phytoplankton: Analysis and parameterization, *Journal of Geophysical Research*, *100* (C7), 13,321-13,332, 1995.

Bricaud, A., and D. Stramski, Spectral absorption coefficients of living phytoplankton and nonalgal biogenous matter: a comparison between the Peru upwelling area and the Sargasso Sea, *Limnology and Oceanography*, *35* (3), 562-582, 1990.

Bukata, R.P., J.H. Jerome, K.Y. Kondratyev, and D.V. Pozdnyakov, Satellite monitoring of optically-active compounds of inland waters: an essential input to regional climate impact studies, *Journal Great Lakes Research*, *17*, 470-478, 1991.

Cannizzaro, J.P., and K.L. Carder, Estimating chlorophyll a concentrations from remote-sensing reflectance data in optically shallow waters, *Remote Sensing of Environment*, 2005 (submitted).

Cannizzaro, J.P., K.L. Carder, F.R. Chen, J.J. Walsh, Z.P. Lee, and C. Heil, A novel optical classification technique for detection of red tides in the Gulf of Mexico: application to the 2001-2002 bloom event, in *Florida Fish and Wildlife Conservation Commission and Intergovernmental Oceanographic Commission of UNESCO*, edited by J.H.L. K.A. Steidinger, C.R. Tomas, G.A. Vargo, pp. 4, Intergovernmental Oceanographic Commission of UNESCO, St. Pete Beach, FL, 2002.

Carder, K.L., J.P. Cannizzaro, F.R. Chen, and Z.P. Lee, MODIS Semi-Analytic Algorithm for IOP, in *Reports of the International Ocean-Colour Coordinating Group, No. 10*, edited by Z.P. Lee, accepted.

Carder, K.L., F.R. Chen, Z.P. Lee, S.K. Hawes, and D. Kamykowski, Semi-analytic Moderate-Resolution Imaging Spectrometer algorithms for chlorophyll *a* and absorption with bio-optical domains based on nitrate-depletion temperatures, *Journal of Geophysical Research*, *104* (C3), 5403-5422, 1999.

Carder, K.L., S.K. Hawes, K.A. Baker, R.C. Smith, R.G. Steward, and B.G. Mitchell, Reflectance model for quantifying chlorophyll a in the presence of productivity degradation products, *Journal of Geophysical Research*, *96* (C11), 20,599-20,611, 1991.

Carder, K.L., and R.G. Steward, A remote-sensing reflectance model of a red-tide dinoflagellate off west Florida, *Limnology and Oceanography*, *30* (2), 286-298, 1985.

Carder, K.L., R.G. Steward, G.R. Harvey, and R.B. Ortner, Marine humic and fulvic acids: their effects on remote sensing of ocean chlorophyll, *Limnology and Oceanography*, *34* (1), 68-81, 1989.

Carder, K.L., R.G. Steward, J.H. Paul, and G.A. Vargo, Relationships between chlorophyll and ocean color constituents as they affect remote-sensing reflectance models, *Limnology and Oceanography*, *31* (2), 403-413, 1986.

Doerffer, R., and J. Fisher, Concentrations of chlorophyll, suspended matter, and gelbstoff in case II waters derived from satellite coastal zone color scanner data with inverse modeling methods, *Journal of Geophysical Research*, *99*, 7475-7466, 1994.

Esaias, W., M. Abbott, I. Barton, O.B. Brown, J.W. Campbell, K.L. Carder, D.K. Clark, R.H. Evans, F.E. Hoge, H.R. Gordon, W.M. Balch, R. Letelier, and P.J. Minnett, An overview of MODIS capabilities for ocean science observations, *IEEE Trans. Geosci. Remote Sens.*, *36*, 1250-1265, 1998.

Gordon, H.R., O.B. Brown, R.H. Evans, J.W. Brown, R.C. Smith, K.S. Baker, and D.K. Clark, A semianalytic radiance model of ocean color, *Journal of Geophysical Research*, *93* (D9), 10,909-10,924, 1988.

Gordon, H.R., D.K. Clark, J.W. Brown, O.B. Brown, R.H. Evans, and W.W. Broenkow, Phytoplankton pigment concentrations in the Middle Atlantic Bight: comparison of ship determinations and CZCS estimates, *Applied Optics*, *22* (1), 20-36, 1983.

Gordon, H.R., and M. Wang, Retrieval of water-leaving radiance and aerosol optical thickness over the oceans with SeaWiFS: A preliminary algorithm, *Applied Optics*, *33*, 443-452, 1994.

Hoepffner, N., and S. Sathyendranath, Determination of the major groups of phytoplankton pigments from the absorption spectra of total particulate matter, *Journal of Geophysical Research*, *98* (C12), 22,789-22,803, 1993.

Holm-Hansen, O., C.J. Lorenzen, R.W. Holmes, and J.D.H. Strickland, Fluorometric determination of chlorophyll, *J. Cons. Perm. Int. Explor. Mer*, *30* (1), 3-15, 1965.

Hu, C., K.L. Carder, and F.E. Müller-Karger, Atmospheric correction of SeaWiFS imagery over turbid coastal waters: a practical method, *Remote Sensing of Environment*, *74*, 195-206, 2000.

Jerlov, N.G., *Marine Optics*, Elsevier, New York, 1976.

Kiefer, D.A., and J.B. SooHoo, Spectral absorption by marine particles of coastal waters of Baja California, *Limnology and Oceanography*, *27* (3), 492-499, 1982.

Kirk, J.T.O., Light capture by aquatic plants, in *Light and Photosynthesis in Aquatic Ecosystems*, edited by J.T.O. Kirk, pp. 201-218, Cambridge University Press, Cambridge, 1994.

Kishino, M., M. Takahashi, N. Okami, and S. Ichimura, Estimation of the spectral absorption coefficients of phytoplankton in the sea, *Bulletin of Marine Science*, *37* (2), 634-642, 1985.

Lee, Z., Visible-infrared remote-sensing model and applications for oceanic waters, Ph.D. dissertation thesis, University of South Florida, St. Petersburg, Fla., 1994.

Lee, Z., K.L. Carder, R.F. Chen, and T.G. Peacock, Properties of the water column and bottom derived from Airborne Visible Infrared Imaging Spectrometer (AVIRIS) data, *Journal of Geophysical Research*, *106* (C6), 11,639-11,651, 2001.

Lee, Z., K.L. Carder, and K. Du, Effects of molecular and particle scatterings on the model parameter for remote-sensing reflectance, *Applied Optics*, *43* (25), 4957-4964, 2004.

Lee, Z., K.L. Carder, C. Mobley, R.G. Steward, and J.S. Patch, Hyperspectral remote sensing for shallow waters: I. A semi-analytical model, *Applied Optics*, *37* (27), 6329-6338, 1998.

Lee, Z., K.L. Carder, C.D. Mobley, R.G. Steward, and J.S. Patch, Hyperspectral remote sensing for shallow waters: 2. Deriving bottom depths and water properties by optimization, *Applied Optics*, *38* (18), 3831-3843, 1999.

Lee, Z., K.L. Carder, T.G. Peacock, C.O. Davis, and J.L. Mueller, Method to derive ocean absorption coefficients from remote-sensing reflectance, *Applied Optics*, *35* (3), 453-462, 1996.

Letelier, R.M., and M.R. Abbott, An analysis of chlorophyll fluorescence algorithms for the Moderate Resolution Imaging Spectrometer (MODIS), *Remote Sensing of Environment*, *58*, 215-223, 1996.

Lewis, M.R., M. Carr, G. Feldman, W. Esaias, and C. McClain, Influence of penetrating solar radiation on the heat budget of the equatorial Pacific ocean, *Nature*, *347*, 543-545, 1990.

Maffione, R.A., and D.R. Dana, Instruments and methods for measuring the backward-scattering coefficient of ocean waters, *Applied Optics*, *36* (24), 6057-6067, 1997.

Maritorena, S., D.A. Siegel, and A.R. Peterson, Optimization of a semi-analytical ocean color model for global-scale applications, *Applied Optics*, *41* (15), 2705-2714, 2002.

Marra, J., T. Dickey, W.S. Chamberlin, C. Ho, T. Granata, D.A. Kiefer, C. Langdon, R.C. Smith, K.S. Baker, R.R. Bidigare, and M. Hamilton, Estimation of seasonal primary production from moored optical sensors in the Sargasso Sea, *Deep-Sea research*, *97*, 7399-7412, 1992.

Millie, D.F., O.M. Schofield, G.J. Kirkpatrick, G. Johnsen, P.A. Tester, and B.T. Vinyard, Detection of harmful algal blooms using photopigments and absorption signatures: A case study of the Florida red tide dinoflagellate, *Gymnodinium breve*, *Limnology and Oceanography*, *42* (5), 1240-1251, 1997.

Mitchell, B.G., Coastal zone color scanner retrospective, *Journal of Geophysical Research*, *99*, 7291-7292, 1994.

Mobley, C.D., *Light and water: radiative transfer in natural waters*, 592 pp., Academic Press, San Diego, 1994.

Morel, A., Optical properties of pure water and pure sea water, in *Optical Aspects of Oceanography*, edited by N.G. Jerlov, and E.S. Nielsen, pp. 1-24, Academic Press, London, 1974.

Morel, A., and D. Antoine, Heating rate within the upper ocean in relation to its bio-optical state, *Journal of Physical Oceanography*, *24*, 1652-1665, 1994.

Morel, A., and L. Prieur, Analysis of variations in ocean color, *Limnology and Oceanography*, *22* (4), 709-722, 1977.

Nelson, J.R., and C.Y. Robertson, Detrital spectral absorption: laboratory studies of visible light effects on phytodetritus absorption, bacterial spectral signal, and comparison to field measurements, *Journal of Marine Research*, *51*, 181-207, 1993.

Neumann, A., H. Krawczyk, and T. Walzel, A complex approach to quantitative interpretation of spectral high resolution imagery, in *Third Thematic Conference on Remote Sensing for Marine and Coastal Environments*, Seattle, USA, 2000.

O'Reilly, J.E., S. Maritorena, B.G. Mitchell, D.A. Siegel, K.L. Carder, S.A. Garver, M. Kahru, and C. McClain, Ocean color chlorophyll algorithms for SeaWiFS, *Journal of Geophysical Research*, *103* (C11), 24,937-24,953, 1998.

Platt, T., and S. Sathyendranath, Oceanic primary production: estimation by remote sensing at local and regional scales, *Science*, *241*, 1613-1620, 1988.

Pope, R., and E. Fry, Absorption spectrum (380-700nm) of pure waters: II. Integrating cavity measurements, *Applied Optics*, *36*, 8710-8723, 1997.

Roesler, C.S., M.J. Perry, and K.L. Carder, Modeling in situ phytoplankton absorption from total absorption spectra in productive inland marine waters, *Limnology and Oceanography*, *34* (8), 1510-1523, 1989.

Siegel, D.A., M. Wang, S. Maritorena, and W. Robinson, Atmospheric correction of satellite ocean color imagery: the black pixel assumption, *Applied Optics*, *39* (21), 3582-3591, 2000.

Signorini, S.R., C.R. McClain, A. Mannino, and S. Bailey, Report on ocean color and carbon study for the South Atlantic Bight and Chesapeake Bay regions, pp. 45, Goddard Space Flight Center, Greenbelt, MD, 2005.

Steward, R.G., and K.L. Carder, Compression of autonomous hyperspectral data, in *Ocean Optics XVI*, Office of Naval Research, Santa Fe, NM, 2002.

Stumpf, R.P., and J.R. Pennock, Remote estimation of the diffuse attenuation coefficient in a moderately turbid estuary, *Remote Sensing of Environment*, *38*, 183-191, 1991.

Yentsch, C.S., Measurement of visible light absorption by particulate matter in the ocean, *Limnology and Oceanography*, *7*, 207-217, 1962.